DOKUZ EYLÜL UNIVERSITY
GRADUATE SCHOOL OF NATURAL AND APPLIED SCIENCES

INVESTIGATION OF COOLING DESIGN SYSTEMS IN LOW PRESSURE CASTING

by
Eren BOZKURT

September, 2019
İZMİR

INVESTIGATION OF COOLING DESIGN SYSTEMS IN LOW PRESSURE CASTING

A Thesis Submitted to the
Graduate School of Natural and Applied Sciences of Dokuz Eylül University
In Partial Fulfillment of the Requirements for the Degree of Master of Science
in Mechanical Engineering, Energy Program

by
Eren BOZKURT

September, 2019
İZMİR

M.Sc THESIS EXAMINATION RESULT FORM

We have read the thesis entitled **"INVESTIGATION OF COOLING DESIGN SYSTEMS IN LOW PRESSURE CASTING"** completed by **EREN BOZKURT** under supervision of **PROF. DR. HÜSEYİN ŞALVARLI** and we certify that in our opinion it is fully adequate, in scope and in quality, as a thesis for the degree of Master of Science.

....

Prof.Dr.Hüseyin ŞALVARLI

Supervisor

Assoc. Prof. Dr. M. Akif EZAN

Jury Member

Assoc. Prof. Dr. Utku ŞENTÜRK

Jury Member

Prof.Dr. Kadriye ERTEKİN

Director

Graduate School of Natural and Applied Sciences

ACKNOWLEDGMENTS

First, I would like to thank my advisor, Prof. Dr. Hüseyin ŞALVARLI, for his patience, effort and support for the completion of the thesis.

Next, I would like to thank the CMS and TÜBİTAK for their scientific and financial support in carrying out this project. Project no: 3180665. I would like to thank Prof. Dr. Aydoğan ÖZDAMAR and Doç. Dr. Utku ŞENTÜRK for their support.

Next, my special thanks to my mother, wife and my daughter, three women in my life; they contributed to my work with their energies and also shared their support in so many ways.

To my father.

Eren BOZKURT

INVESTIGATION OF COOLING DESIGN SYSTEMS IN LOW PRESSURE CASTING

ABSTRACT

Low-pressure die casting is becoming more common day by day due to low mold cost and ease of production. In this study, low-pressure die casting cooling systems were investigated. The types and uses of mold cooling systems were detailed. Generally, air is used as a coolant in low pressure die casting. Air cooling is used to provide directional solidification to prevent casting defects in the casting. The test setup was designed and prepared for the project. This project is conducted as numbered of 3180665 TEYDEB project and supported by TÜBİTAK in Turkey. The rapid cooling of the molds of produced by the low-pressure die casting is important for both the material internal structure and the production time. Hence, the product molds are cooled impinging jets. Different types of cooling systems were tested in the test environment. Nusselt number and heat transfer coefficients (h) were calculated from a single nozzle which is designed Ø4 mm diameter and 6 mm distance to the surface.

Keywords: Low pressure die casting, impinging jet, numerical and experimental study

ALÇAK BASINÇLI DÖKÜMDE SOĞUTMA TASARIM SİSTEMLERİNİN ARAŞTIRILMASI

ÖZ

Düşük kalıp maliyeti ve üretim kolaylığı nedeniyle alçak basınç döküm gün geçtikçe daha yaygın hale gelmektedir. Bu çalışmada, alçak basınçlı döküm soğutma sistemleri incelenmiştir. Kalıp soğutma sistemlerinin çeşitleri ve kullanımları detaylandırılmıştır. Genel olarak, alçak basınçlı dökümde soğutucu olarak hava kullanılır. Hava, yönlendirilmiş katılaşma sağlayarak döküm hatalarını önlemede kullanılır. Test düzeneği, proje için tasarlanmış ve hazırlanmıştır. Bu proje 3180665 TEYDEB projesi olarak gerçekleştirilmiş ve TÜBİTAK tarafından Türkiye'de desteklenmiştir. Alçak basınçlı kalıp dökümünde, kalıpların hızlı soğutulması hem malzemenin iç yapısı hem de üretim süresi için önemlidir. Bu nedenle, ürün kalıpları için jet soğutucular kullanılır. Test ortamında farklı tip soğutma sistemleri test edilmiştir. Nusselt sayısı ve ısı transfer katsayıları (h), Ø4 mm çapında ve yüzeye 6 mm mesafede tasarlanmış tek nozülden hesaplandı.

Anahtar Kelimeler: Alçak basınçlı döküm, çarpan jeti, sayısal ve deneysel çalışma

CONTENTS

Page

LIST OF FIGURES

Page

LIST OF TABLES

Page

CHAPTER ONE
INTRODUCTION

Transportation plays an important role in economic and social life. Countries population and transport activity increase very fast. The number of cars and activities are predicted to be double between 2005 and 2050. Unfortunately, transportations and vehicles are becoming the greatest reason for pollution that human-made. Especially, poor combustion system of fossil and biomass are contributing to air pollution. Non-OECD countries will have two-thirds of the global vehicle in 2050. But the technological improvements of vehicles have not been developed rapidly enough to catch the number of vehicles growth in the cities. United Nations Environment Programme (UNEP) has prepared detail information about air pollution effect and reason (UNEP, 2019). Most of the air pollution in cities is caused by vehicle emissions. Decreasing vehicle weight is the key to air pollution (Helms, & Lambrecht, 2006). Vehicle weighting is discussed as one way to reduce energy consumption. Nowadays, many studies are carried out about the reduction of car weight.

Aluminum components have been used in many industries since the early 20th century. Nowadays, most parts of the car are made aluminum alloy because of having good formability, high strength, better fatigue and impact performance, high corrosion performance, malleable and elastic structure. Aluminum alloys are used for cylinder heads, brake components, suspension components, brake calipers, bumpers and wheels. Engineers and experts try to reduce vehicle weight and compare different processes for manufacturing these parts because of economical and strength. In the case of wheels, end-users demand more aesthetic wheel and also manufacturers want lightweight. For these reasons, the design of wheels and molds are getting complex and difficult day by day. Modern aluminum alloy wheels allow to making lightweight.

There are many ways to produce automotive parts. Die-cast processes (High pressure die casting, low-pressure die casting, etc.) are one of the most widely used and refer to forming molten metal. But we will discuss the well-known casting process, Low-Pressure Die Casting (LPDC).

1.1 Low pressure die casting

The low-pressure die casting (LPDC) is a widely used casting process to produce automotive wheels. The LPDC system is shown in Figure 1.1. LPDC Machine could be classified into 4 main groups;

a) Main parts of mold (upper mold and bottom core)
b) Four side blocks
c) Cooling systems
d) Standard parts (plate, bushing, nut, bolt)

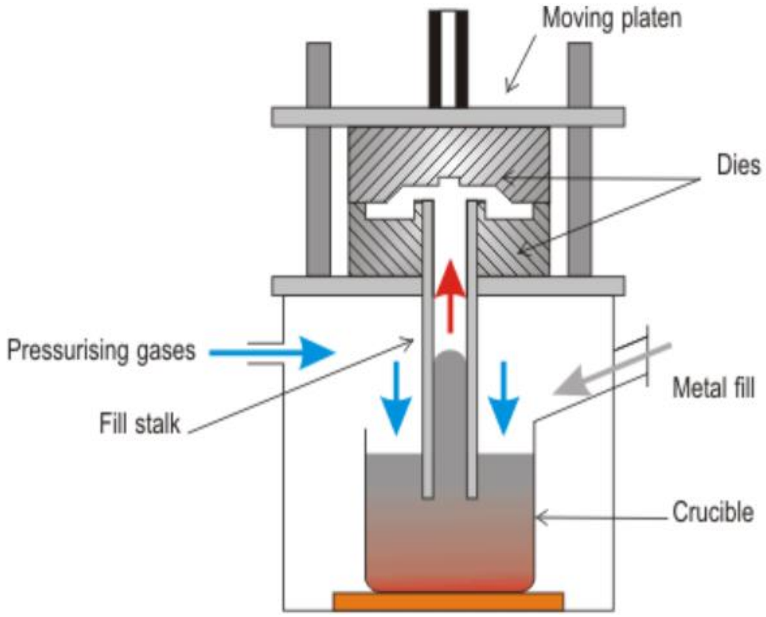

Figure 1.1 Low pressure casting machine (L&ES, 2014)

The crucible is filled with molten metal when the system is started; molten metal is raised by dry air or an inert gas (esp. nitrogen gases) with relatively low pressure (usually from 600 to 1000 mbar). The molten metal rises the riser-tube and fills the mold cavity from the casting gate. The pressure increases until the mold cavity filled with the molten metal. The time of the solidification depends on the geometry of the wheel and filling speed of the mold cavity. The stages of the filling processes are shown in Figure 1.2 (Solian, Leslie, Langnau, Pablo & Fernandez, 2016).

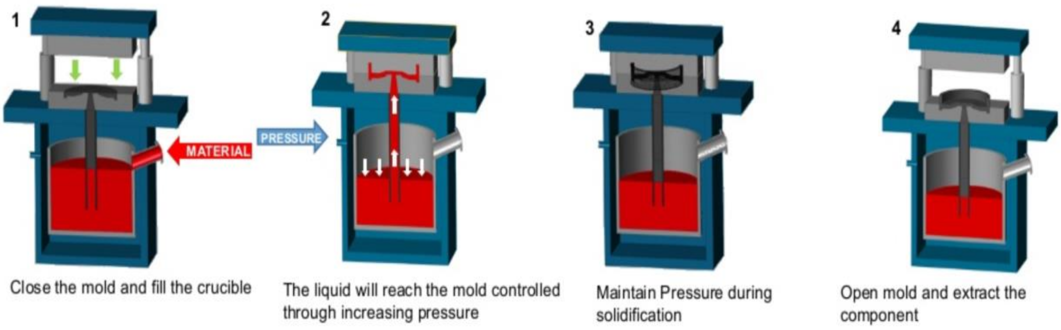

Figure 1.2 The stages of the filling processes (Solian, Leslie, Langnau, Pablo & Fernandez, 2016)

Process Steps:

1- LPDC mold is prepared and closed
2- Air pressure is applied to the furnace and molten metal rises up to riser tube (1st stage)
3- Molten metal fills the mold cavity (2nd stage). The die filling takes 10-30 seconds depending on the wheel geometry and pressures used.
4- Pressure is maintained until the casting has solidified (3rd stage)
5- The furnace pressure is reduced to 0 and the molten metal is returned to the furnace.
6- After solidification is completed, then the side blocks are opened and the upper mold moves vertically with the cast wheel because of the thermal contraction of aluminum alloy.
7- The wheel is rejected and the other cycle is started.

Hines (2014) explained furnace pressure, molten metal movement and described molten metal movement in the stalk tube (Equation 1.1). Figure 1.3 shows the LPDC furnace and pressure-time graphic (Joy & Hines, 2004). The molten metal moves by air and rises in the stalk tube. After this process, the mold is filled with molten metal. Height of molten metal in the stalk tube is calculated with;

$$\Delta P = \rho g \Delta h [1 + (\frac{d}{D})^2] \quad (1.1)$$

In this equation, ΔP is pressure, g is acceleration of gravity (m/s^2), ρ is the density of the working fluid (here is the molten metal, kg/m^3), Δh is distances between surface of the molten metal rised in the stalk tube and surface of the molten metal in the furnace, d is diameter (here is the diameter of stalk, m) and D is diameter (here is the diameter of furnace, m).

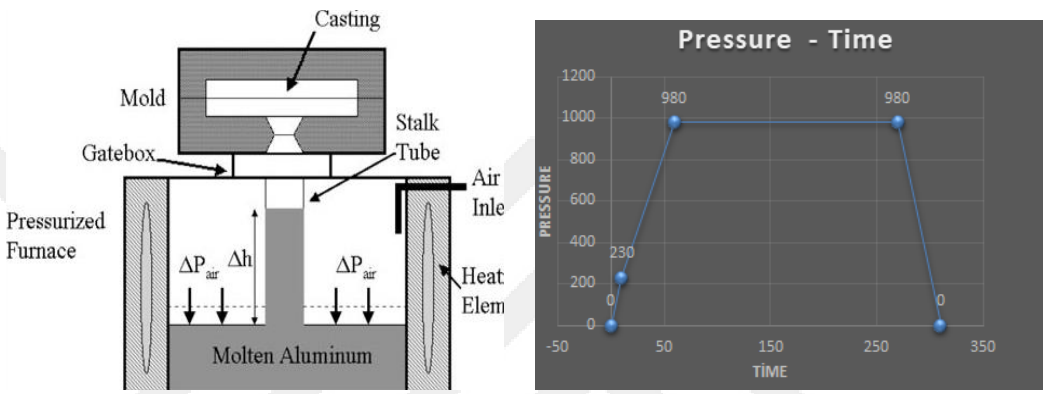

Figure 1.3 LPDC furnace and pressure-time graphic (Hines, 2004)

1.2 Solidification of molten metal in the mold cavity

Air, water and mist cooling (mixture of the air and water) systems are used as a coolant. In this study, the air cooling system is investigated. Figure 1.4 shows the five-spoke and complex geometry of the wheel which occurs rim, spokes and hub. The wheel is connected to the car by means of holes in the hub area. So, weights of the car and loads are transferred from the hub to inner flange. Both the weight of the car and bending loads are applied to the wheel. Surface of spoke can be designed as a complex to eliminate aesthetic concerns. Therefore, preventing of casting defects are very important for safety and aesthetic concerns.

Figure 1.4 Five-spoke wheel (CMS, 2019)

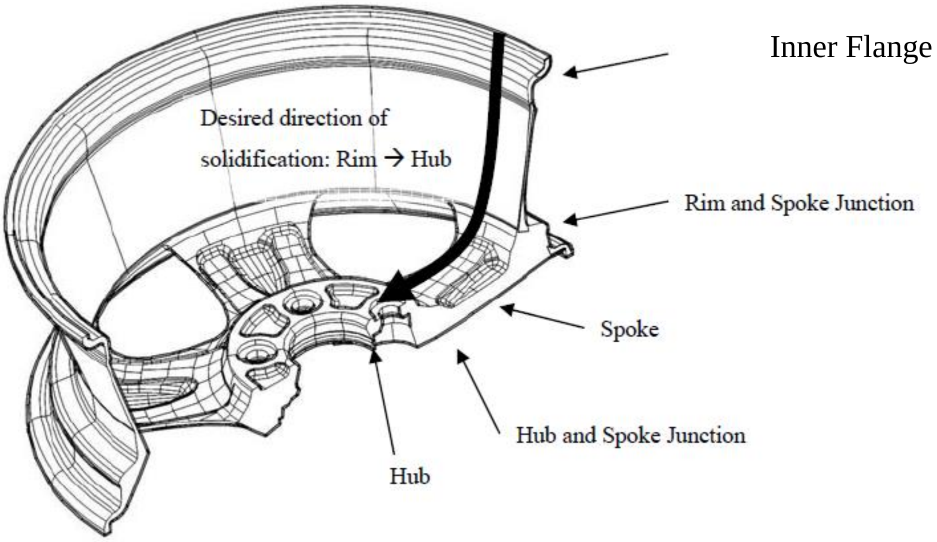

Figure 1.5 Direction of solidification (Lee, 2006)

Figure 1.5 shows the direction of solidification, solidification should be from rim to hub (from inner flange to outer flange). To obtain desired mechanical properties and shape, solidification must be controlled. Referring to Figure 1.6, cooling system can be controlled with starting the cooling system 7, 4-6, 3-5 and 1-2 respectively.

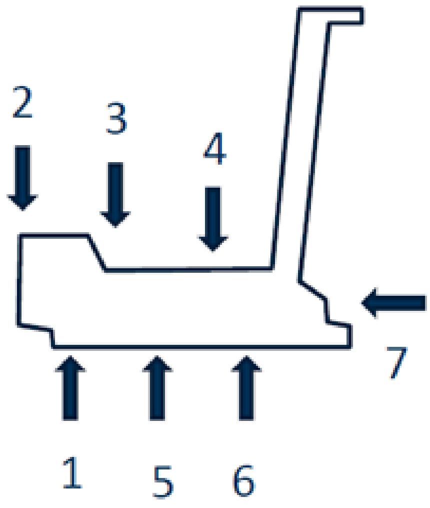

Figure 1.6 Cooling system

The length of the solidification time is dependent on the wheel geometry and temperature of mold must be measured with temperatures sensors near the location in which could be occur casting defects and the random surface of the mold for controlling the cooling system. Cooling systems are designed from trial and error methods and results of casting simulation. Nowadays, simulation engineers work for improving casting simulation results because of time-saving. Trial and error methods take a long time and cause high costs. During solidification, loss of directional control of the solidification can cause casting problems. To achieve directional solidification, the cooling system must be checked with flow-meters.

For many years, many studies are carried about heat transfer between molten metal-mold and mold-surround. The motion of molten metal is described in Figure 1.2. And we can simply classify the casting process in four steps.

Step1. Mould is closed and molten metal rises in the riser-tube. Heat transfer between molten metal-riser tube.

Step2. Mould is filled. Heat transfer between molten metal-mold and from the mold to the environment.

Step3. Maintain pressure during solidification. Heat transfer from the side and bottom dies to the environment, heat transfer from the wheel to the top die and to the environment and heat transfer from the top die to the environment.

Step4. Open mold, and extract the wheel. Heat transfer from the side, bottom and top dies to the environment.

In Figure 1.7 shows the heat transfer between molten metal-mold (Interface Type) heat transfer, mold-surround (Environment type).

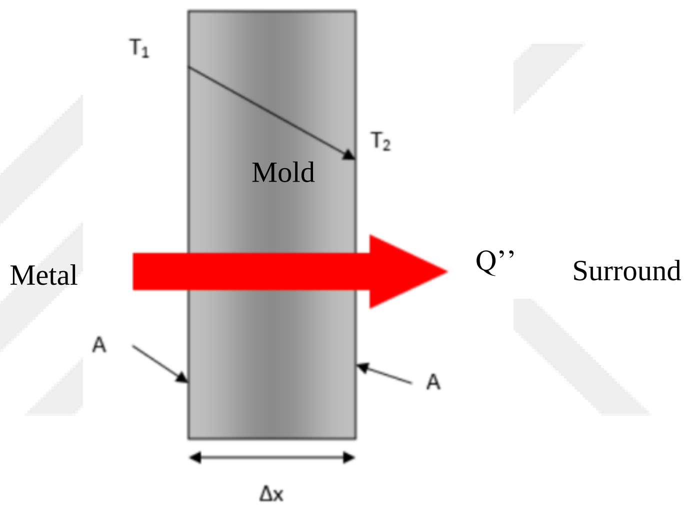

Figure 1.7 Heat transfer between mold and metal

Molten metal solidification in a mold is affected many factors like mold temperature, molten metal temperature, mold materials (physical, chemical and thermal properties), mold coatings, types of cooling (air, water, and mist) and cooling flow rates.

Figure 1.8 shows the air gap conditions between mold and metal. Due to the gaps between the metal and the mold, the contact could be made from different regions. Regional temperature differences are caused because of the air gap. It is seen that the heat transfer is made up of contact zones. On the other hand, an exaggerated air gap is shown in Figure 1.8.b. heat transfer in these regions is considered zero. Region of A is represented the molten metal and region of B is represented the mold.

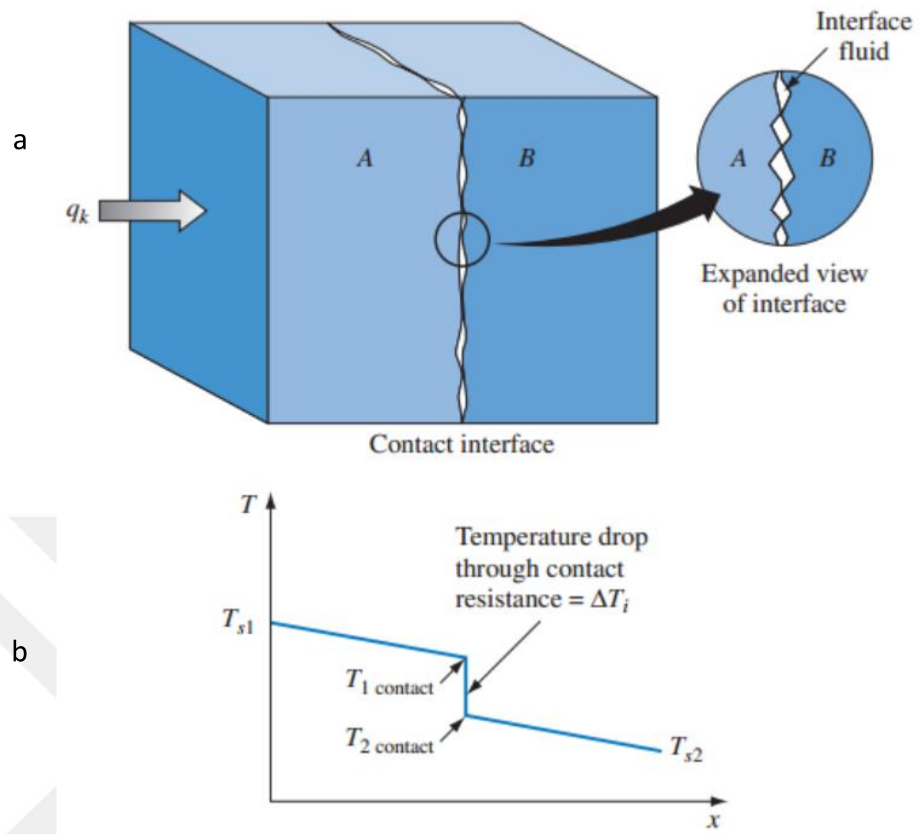

Figure 1.8 View of air gap (Wei, 2014)

1.3 Casting Defects

The wheel is critical for automobile safety and visuality. The mechanical, internal structure quality and cosmetic tests are quite difficult. Casting defects have been classified as porosity, oxide film, and hot cracks (Zhang, Cockcroft, Maijer, Zhu & Phillion, 2005).

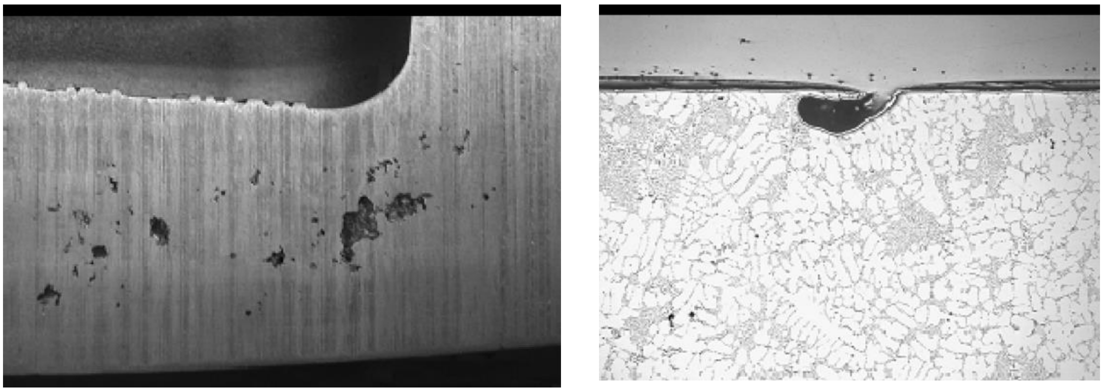

a) b)

Figure 1.9 Porosities a) macro-porosity or shrinkage b) micro-porosity (Zhang, Cockcroft, Maijer, Zhu & Phillion, 2005)

Macro-porosity (shrinkage, Figure 1.9 a) occurs when there is an encapsulation of liquid because of solidification path has been changed. The most common location is found in the region where spoke and rim intersect. Casting shrinkage is occurred because of the loss of directional solidification. Macro-porosity or shrinkage affects fatigue and impact performance of the wheel. So, the load of bearing capacity of the wheel is dramatically affected.

Another defect problem micro-porosity (<~300 μm in diameter, Figure 1.9.b), appears on the surface or near-surface. The fact that the problem is on the surface causes visual problems. Hydrogen is the reason for the formation of micro-porosity. Aluminum gets hydrogen from the ambient air. Fast cooling process solves micro-porosity caused by hydrogen.

Oxide films occur when a molten metal state on the surface of the metal. Oxide films are related to flow characteristics. Turbulence may occur when filling the cavity of the die with molten metal. The way to prevent turbulence is to reduce the speed of filling and also change die or wheel design. Another way is filtering molten metal reduces oxide films and increase molten quality.

Figure 1.10 shows the Fish-Bone diagram of casting defects. If the mold and time section are examined in detail, casting defects are caused by parameters of the cooling system.

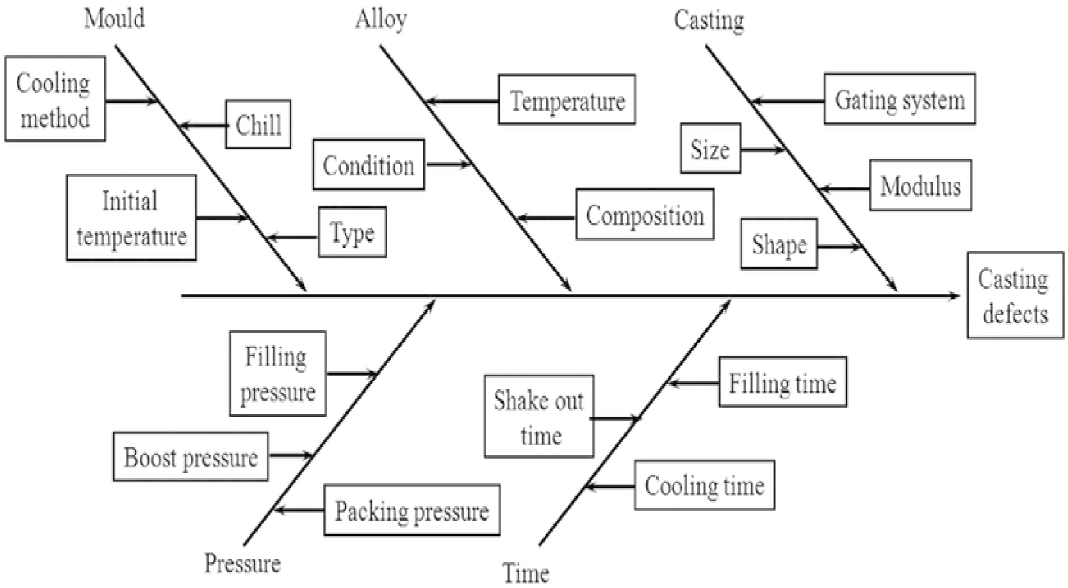

Figure 1.10 Fish-bone diagram of casting defects (Wang, 2014)

In conclusion, there are some ways to prevent defects of casting defects. The developing of materials science also helps to improve and solve defects. If material science and design are used together, the solution can be very impressive. The modifications of mold and wheel designs, especially the cooling designs, will help directional solidification. If the mathematical modeling of cooling design is prepared, the processing times will be reduced.

1.4 Problem Statement

The most effective way to reduce the negative conditions described in Sections 1.2 and 1.3 is through the effective use of the cooling system. With today's technologies, a controlled cooling system is suggested to ensure directed solidification. Water, air and mist fluent are used for the cooling systems. If the single-phase cooling system is desired, jet impingement is the best way to cool, because maximum heat transfer is obtained by air cooling systems. The air used for the cooling system reaches high speeds. Therefore, it is called jet impingement. Jet impingement cooling system is used in many industries due to achieving high heat transfer coefficients. Jet impingement is used for cooling of electronics parts, turbine blades and casting process; drying of paper, textile and drilling process; cooling/heating of glass industries (Anuj, Shukla & Dewan, 2017).

In Figure 1.11 cooling channels are shown with red-colored. Number and locations of cooling channels are changed due to wheel geometries. The location, capacity, and number of cooling system can be changed due to X-ray defects (porosity and shrinkage) occurring during casting analyzes and trial castings.

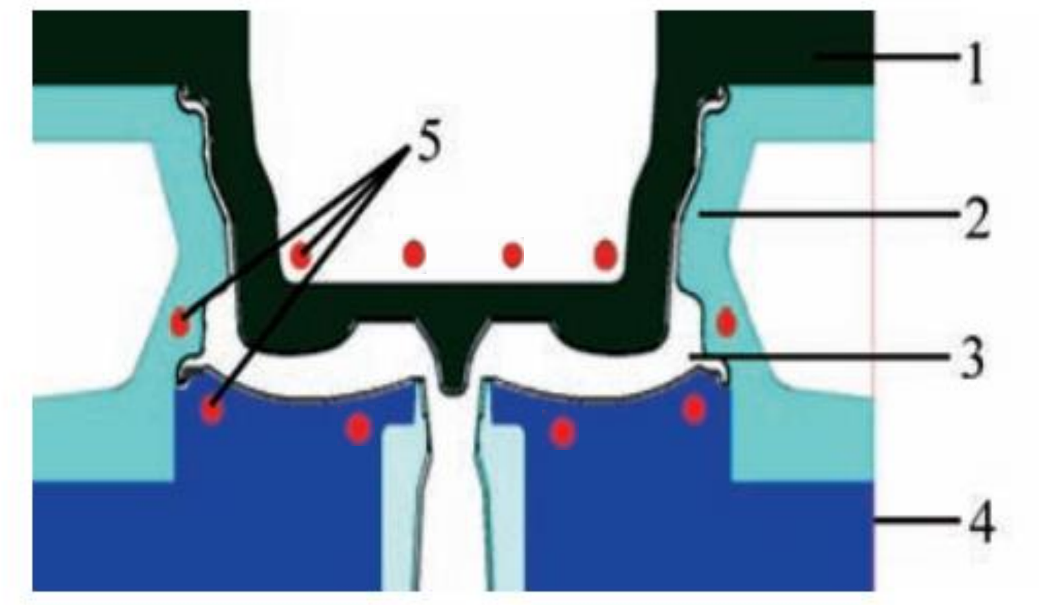

Figure 1.11 Location of cooling channels 1-top mold 2-side mold 3-casting 4-lower mold 5-cooling system (Guofa, Xiangyu, Kuangfei & Hengzhi, 2009)

Scientific and industrial studies have been carried out about jet impingement. The configurations of the nozzle (types, lengths, structures and shapes), air velocity, distance and angle between surface and nozzle are the subject of the study according to the area where the cooling system is used. Also, single and multiple jets and impingement surface on both flat and convex are investigated about heat transfer.

1.5 Physical Mechanism of Mold Cooling System

In order to increase the efficiency of the heat transfer, forced convection is applied to the mold by a compressor. Air is transferred from the compressor to mold surface by a pipe which is categorized as internal forced convection. Figure 1.12 shows the general view of air cooling system.

The air is compressed by a compressor. The air is moisturized by high pressure and temperature. Before entering the mold, the air enters the air dryer for reading the pressure and flow values. The humidity of the air is removed because humidity damage electronic devices. After adjusting the temperature of the compressed air, it enters the filters to separate it from the foreign substances that may be contained in the air. After filtering, air is transported to the desired areas with pipes. Finally, after the desired pressure and flow adjustment is made by regulator, it is directed to the mold.

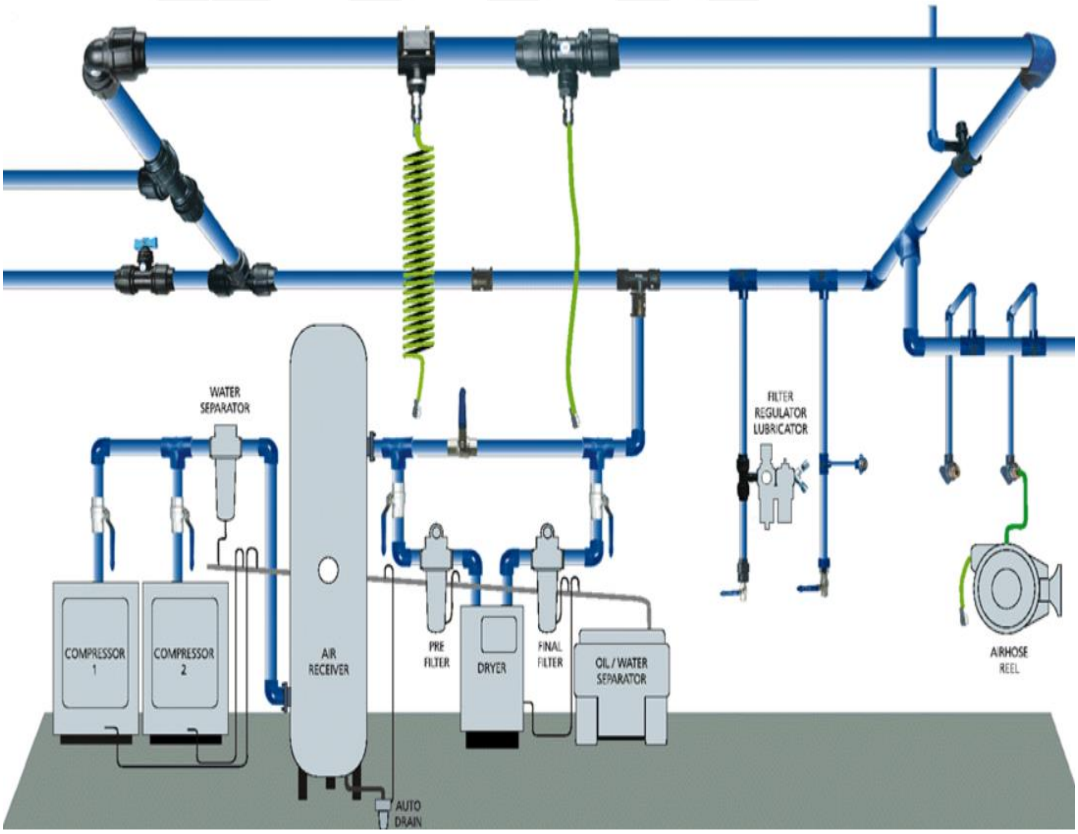

Figure 1.12 General view of air cooling system (Aircompressor, 2016)

Conduction, convection and radiation are the three basic heat transfer mechanisms. Conduction is always heat transfer through a solid. On the other hand, in the liquid or gas environment, the heated liquid or gas is in continuous motion. The heated liquid or gas rises and is replaced by colder liquid or gas. This cycle results in a continuous circulation pattern and heat is transferred to cooler areas.

Convection heat transfer is complicated because of the fluid motions and also fluid motion enhanced heat transfer. Therefore in liquids and gases, convection is usually the most efficient way to transfer heat. Convection heat transfer depends on the fluid properties;

Table 1.1 The properties of fluid which affect the convection heat transfer

dynamic viscosity	μ	Pa s
thermal conductivity	k	W/(m K)
density	ρ	kg/m^3
specific heat	c_p	J/(kg K)
fluid velocity	V	m/s

Convection heat transfer also depends on geometry and roughness of the solid surface, and it is affected by the fluid-flow (turbulent or laminar), too.

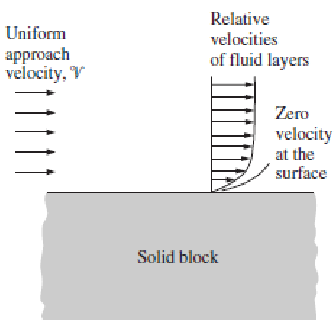

Figure 1.13 Behavior of the fluid flow (Cengel, Cimbala & Turner, 1998)

Figure 1.13 shows the nonporous solid block and behavior of the fluid flow over the solid. The fluid begins to move uniformly on the solid surface. Due to the viscosity (internal resistance of flow) of the fluid, the fluid layer in direct contact with a solid surface "sticks" to the surface and there is no slip. In fluid flow, this phenomenon is known as the no-slip condition. And this phenomenon changes the profile of the fluid layer due to friction between fluid layers (Cengel, Cimbala & Turner, 1998).

When the fluid contacts the solid surfaces, heat transfer occurs until both the same temperatures at the point of contact. Heat transfer can be expressed as;

$$q_{conv} = q_{cond} = -k_{fluid} \frac{\partial T}{\partial y}\bigg|_{y=0} \tag{1.2}$$

In this equation, $(\partial T/ \partial y)_{y=0}$ is the temperature gradient at the surface. Because of the zero velocity in the places where the fluid and surfaces contact each other, heat transfer occurs through conduction between surfaces.

1.6 Literature Review

1.6.1 Classification of Fluid Flows

When we study fluid flows, we also should know the below definitions. These definitions will help us to determine the properties of the fluid used.

1.6.1.1 Viscous and Inviscid Flow

Viscosity is defined as the internal resistance of flow because it occurs when two fluid layers move relative to each other. Viscosity is caused by cohesive forces between the molecules in liquids, and by the molecular collisions in gases. The streams where viscosity is active are called viscous flow. In some flows, this friction is negligible. And this is considered zero, these streams are also called Inviscid flow.

1.6.1.2 Internal and External Flow

Fluid flow is classified as being internal (in a pipe or duct) and external (unbounded flow, like a plate).

1.6.1.3 Compressible and Incompressible Flow

Whether fluids can compress or not is determined by the change in density. During the flow, the density of liquids is constant. Therefore, it is called incompressible flow. On the other hand, the situation for gases is very different. Even changes of 0.01 atm result in a 1 percent change in the density of the atmospheric air.

Generally, the compressibility of the fluid is decided with Mach number. (Mach number is explained at 1.6.2 Dimensionless Number section)

1.6.1.4 Laminar and Turbulent Flow

Figure 1.14 shows the laminar and turbulent flow, and laminar streamlines are parallel to each other. The laminar flow generally occurs when the fluid flows with low velocity (high-viscosity fluids such as oil). On the other hand, for turbulent as shown in Figure 1.14, fluid layers cross and don't move to parallel each other. The turbulent flow occurs when the fluid flows with high velocity (low-viscosity fluids such as air).

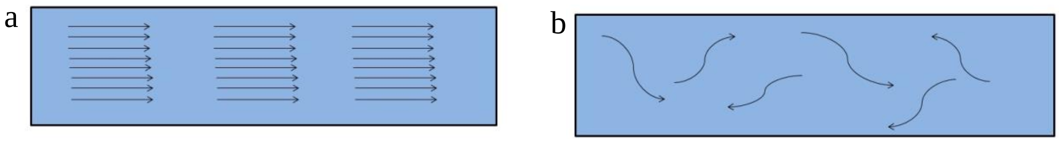

Figure 1.14 Turbulences a) laminar flow b) turbulent flow (Mishra, 2016)

Laminar and turbulent flows are related to Reynolds number. (Reynolds number is explained at 1.6.2 Dimensionless Number section). Figure 1.15 shows the development of the velocity boundary. Laminar and turbulence can occur in the same flow. The laminar flow region continues until the transition region. In the transition region, turbulent flow occurs in some regions, laminar flow occurs in some regions.

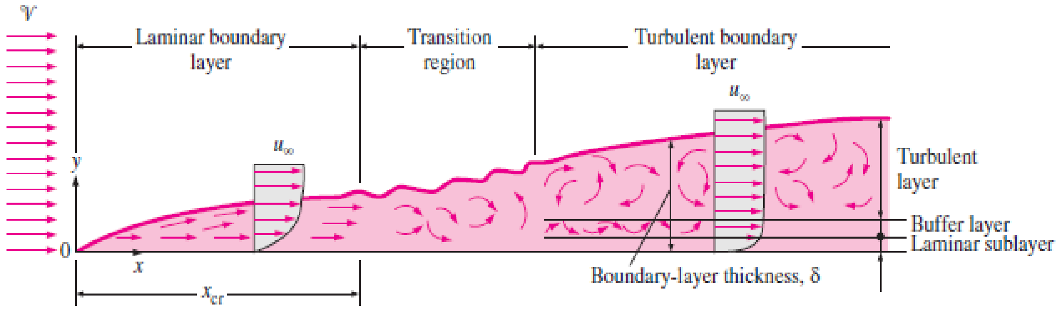

Figure 1.15 Velocity boundary layer development on a flat plate (Cengel, Cimbala & Turner, 1998)

1.6.1.5 Natural and Forced Flow

Unforced and forced flows are related to the flow's initial conditions. If the flow is obtained by means of a compressor, this flow is called forced-flow (Figure1.12). However, if the flow is obtained by natural methods, such as the motion of air which rises when it is heated. Flow is defined as unforced-flow.

1.6.1.6 Steady and Transient (Unsteady Flow)

Steady flow, all fluid flow properties (e.g., velocity, temperature, pressure, and density) are independent of time. The properties, however, may vary from point to point, which means that they could be a function of space. Steady flow does not mean the velocity and accelerations are constant. Flow in a curved pipe or through a nozzle may be steady, but the velocity and/or acceleration are not constant. For unsteady flow, the fluid properties are a function of time.

1.6.1.7 Dimensional Flows (One, Two and Three)

Dimensional flow refers to the number of space coordinated required to describe flow. It appears that any physical flow is generally three-dimensional. But these are difficult to calculate and call for as much simplification as possible. This is achieved by ignoring changes to flow in any of the directions, thus reducing the complexity. It may be possible to reduce a three-dimensional problem to a two-dimensional one, even a one-dimensional one at times.

1.6.2 Dimensionless Numbers

When working with heat transfer, it is necessary to discuss another important issue, dimensionless numbers. Actually, we do not need these numbers when we calculate heat transfer problems. These numbers guide us to compare the information we obtain from different systems with each other. For instance, two different diameters of the pipes are examined. Diameters of the pipe are approved 8 mm and 20 mm. Experimental studies are carried out the diameter of pipe 8mm. The results obtained from this experiment use dimensionless numbers for the comparison of diameter 20 mm. And the results can be examined without the need for experiments with the mathematical calculations.

The most known dimensionless number used for heat transfer is the Reynolds Number. Osborne Reynolds experimented with pipes of different diameters. So now, we can easily decide whether the pipe flow will be laminar or turbulent by using the Reynolds number. The dimensionless numbers we will describe in this section are the most common numbers used in heat transfer:

1.6.2.1 Nusselt Number

In Convection studies, Nusselt number provides a measure of the convection heat transfer at the surface. In the previous section, the no-slip condition is described. Again, this condition is considered and the Nusselt Number is described as;

$$Nu = \frac{hL_c}{k} \tag{1.3}$$

In this equation, h is the heat transfer coefficient (W/(m^2 K)), k is the thermal conductivity of the fluid (W/(m K)) and L_c is the fluid layer of thickness (m).

Heat transfer of convection and also because of fluid layer is motionless, heat is transfer by conduction. Heat flux, in either case, will be;

$$q''_{conv} = h\,\Delta T \tag{1.4}$$

and

$$q''_{cond} = k\,\frac{\Delta T}{L} \tag{1.5}$$

Their ratio gives the Nusselt number.

$$\frac{q''_{conv}}{q''_{cond}} = \frac{h\,\Delta T}{k\,\frac{\Delta T}{L}} = \frac{h\,L}{k} = \mathrm{Nu} \tag{1.6}$$

When the Nusselt number of Nu=1 for a fluid layer represents heat transfer across the layer by pure conduction.

1.6.2.2 Prandtl Number

Prandtl Number is related to the thickness of the thermal and velocity layer. And this number calculated;

$$\mathrm{Pr} = \frac{Molecular\ diffisuvity\ of\ momentum}{Molecular\ diffusity\ of\ heat} = \frac{\mu\,c_p}{k} \tag{1.7}$$

In this equation, μ is dynamic viscosity of the fluid (Pa s = N s/m^2), k is thermal conductivity of the fluid (W/(m K)), c_p is specific heat of the fluid (J/(kg K)), ρ is density of the fluid (kg/m^3).

Table 1.2 shows the range of the Prandtl Numbers. When the Prandtl Numbers=1, momentum and heat dissipate through the fluid at about the same rate. When Pr<1, heat diffusivity is bigger than velocity diffusivity. When Pr>1, than velocity diffusivity is bigger than heat diffusivity.

Table 1.2 Prandtl numbers for common fluids

Fluid	**Pr**
Liquid metals	0.004-0.030
Gases	0.7-1.0
Water	1.7-13.7
Light organic fluids	5-50
Oils	50-100 000
Glycerin	2000-100 000

1.6.2.3 Reynolds Number

The inertia forces and viscous forces ratio affect the behavior of fluid-flow. Reynolds number is defined as below;

$$\mathrm{Re} = \frac{Inertial\ forces}{Viscous\ forces} = \frac{\rho\, V\, L}{\mu} \tag{1.8}$$

In this equation, V is the characteristic velocity of fluid (m/s), L is the characteristic length, μ is dynamic viscosity of the fluid (Pa s = N s/m^2), ν is kinematic viscosity of the fluid ($\nu = \mu/\rho$, m^2/s), ρ is the density of the fluid (kg/m^3).

In pipe flow, for instance, V is the mean velocity of fluid flow through pipe and L is the pipe diameter.

In a normal liquid flow, small turbulence occurs. As long as viscous forces dominate, these turbulences are under control. As inertia forces grow, viscosity can no longer maintain order and these little turbulences begin to grow.

The thickness of the boundary value is another significant amount affected by the Reynolds number. As the Reynolds number increases, the viscous layer is compressed to a smaller distance than the surface.

According to Reynolds number, in-pipe flow is classified as below;

Re < 2000	Laminar Flow
2000 < Re < 4000	Transition Flow (either laminar or turbulent)
Re > 4000	Turbulent Flow

1.6.2.4 Mach Number

The Mach number is the ratio of flow velocity after a certain limit of the sounds speed. The Mach number due to the local speed of sound is dependent on the surrounding mediums in specific temperature and pressure. Mach number can be expressed:

$$M = \frac{V_{object}}{V_{sound}} \tag{1.9}$$

In this equation, V_{object} is the velocity of the source relative to the medium (m/s) and V_{sound} is the speed of sound in the medium (m/s) and can be expressed;

$$V_{sound} = 331 + 0.6\,T \tag{1.10}$$

In this equation, *T (°C)* is the ambient temperature (Moayedinia, 2014).

A flow can be determined as an incompressible or compressible flow with the help of the Mach number. The Mach number is termed as a dimensionless number because it is a ratio of two speeds. When the Mach number of flow is less than 0.3, the density changes are under about 5 percent. And this flow is called incompressible flow. The velocity of sound in air at room temperature is 346 m/s (The velocity of sound in air at 20°C 343 m/s). Therefore, the compressibility effects of air can be neglected at speeds under 100 m/s (Cengel, Klein & Beckman, 1998).

1.6.2.5 Grashof Number

Grashof number, Gr, represents the ratio between the buoyancy force due to spatial variation in fluid density (caused by temperature differences) to the restraining force due to the viscosity of the fluid.

$$Gr = \frac{g\beta(T_{wall} - T_{\infty})D_h^3}{\upsilon^2} \tag{1.11}$$

In this equation, υ is kinematic viscosity of the fluid ($\nu = \mu/\rho$, m^2/s), g is acceleration due to the gravity (9.8 m^2/s), T_{wall} is the cooling channel surface temperature, T_{∞} is the sink or bulk temperature of air and β is the volume coefficient of expansion for ideal gases ($\beta=1/T_{film}$).

1.6.3 Heat Transfer

In figure 1.16 the efficiencies of the different cooling systems are shown. (Lasance, 1997). In this study, forced air system is researched. Different amounts and different types of fluids are used according to the directed solidification. If air is used as a fluid, the flow rate should be increased if the efficiency of the cooling system is to be increased. In order to increase the airflow, the diameter of the pipe used is increased or the pressure of the system is increased. Work has been carried out with different cooling systems. (Moayedinia, 2014) studied water, air and mist cooling on the wheel mold and described the heat transfer in the cooling channels of the low-pressure die casting process.

Another important issue affecting the heat transfer is the surface on which the fluid is applied. Baughn et al., 1991, Chandramohan et al., 2017, and Zukowski, 2013, were studied on flat surfaces, Dharavath and Chakraborty, 2013, were studied on inclined surfaces and Azimi et al. 2015, were studied on the concave surfaces (Baughn, Hechanova, & Yan, 1991).

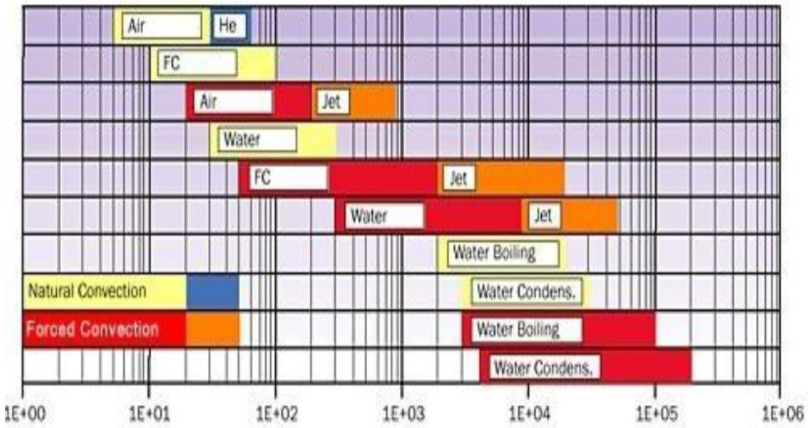

Heat Transfer Coefficient

Figure 1.16 The efficiency of the different cooling systems (Lasance, 1997)

The heat transfer coefficient is affected with nozzle type, numbers, diameter (D) and distances from surfaces (H). Marzec & Marzec (2014), Royne & Dey (2006), Koseoglu & Baskaya (2010), Whelan & Robinson (2009), were studied different nozzle geometries. Abdullah et al. (2018), were studied about number of nozzle.

In Figure 1.17 different kind of cooling pipes which are used for low pressure die casting wheel manufacturing are shown. Nozzle numbers and types vary from place to place. Each cooling pipe has different studies topics.

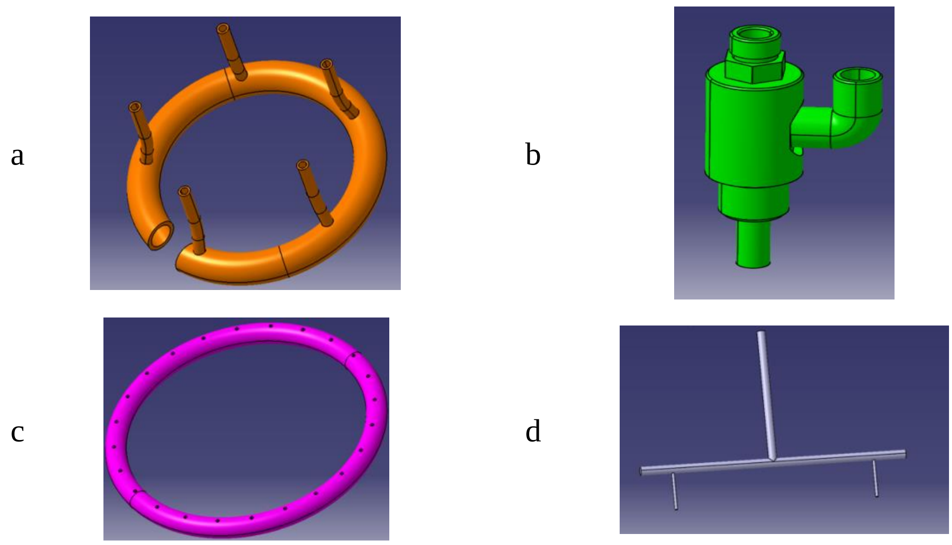

Figure 1.17 Cooling pipes a) nozzle b) single c) holes d) side block

As shown in Figure 1.17 the number of nozzles can be single or multiple. Furthermore, the surface may be concave or flat. In the cooling system shown in Figure 1.18, compressed air is transmitted to the mold surface by means of multiple nozzles. Forced convection is applied to the mold by pipes and compressors. In this system, heat transfer is affected by airflow, pipe outlet diameter and distance between pipe-mold surfaces.

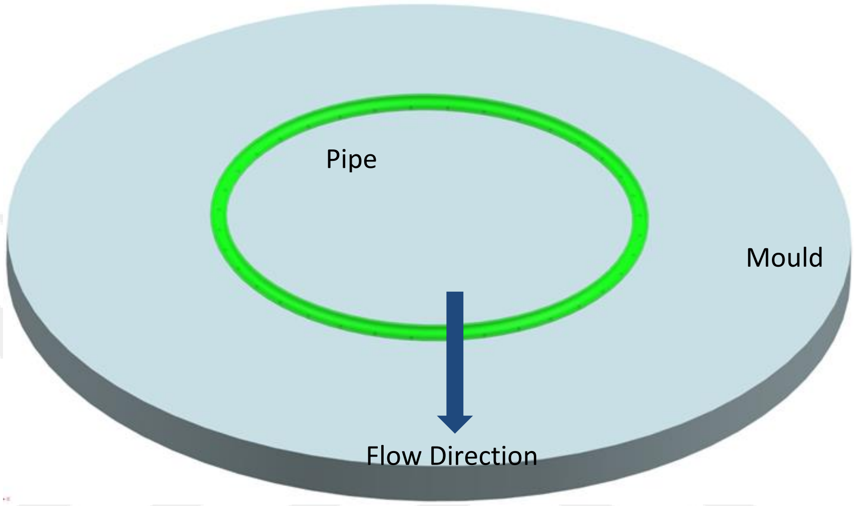

Figure 1.18 Multi nozzle pipe

Figure 1.19 shows one single nozzle. Generally, the fluid is transmitted from the diameter D to the surface H at the velocity V. The flow consists of 3 regions which as described free jet region, stagnation region and wall jet region. The fluid moves in the free zone after it exits the nozzle and has not yet been influenced by the impingement. Thus, it acts like a free submerged jet or free jet region. During this movement, the surrounding fluid begins to enter this area and begins to slow down the speed of the jet velocity with an increase in the total mass flow rate. The jet fluid begins to lose its kinetic energy, and the velocity profile begins to expand. As it progresses towards the impact surface, the edges of the velocity profile continue to shrink. Thus, a non-uniform radial velocity profile develops within the jet. Jet fluid outlet conditions and geometry of the nozzle affect the potential core. Developing zones starts after the potential core because of the large shear stresses at the boundary of jet fluids. Shear stresses affect the axial velocity profile. After the developing zones, fully developed zones start because the fully developed velocity profile is obtained (Jambunathan, Lal, Moss & Button, 1992).

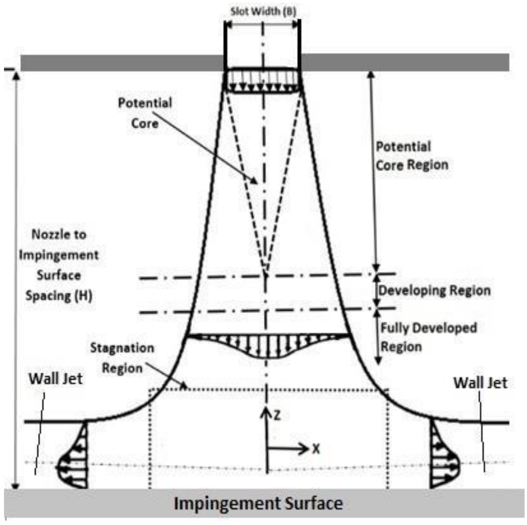

Figure 1.19 Different regions of a jet impingement flow (Jambunathan, Lal, Moss & Button, 1992)

Also, impinging jet can be separated as a submerged jet and free surface jet. In Figure 1.20, different types of impingements are shown. In case of submerged impinging jets liquid has the same structure as the environment flowing through the nozzle. On the other hand, in case of free surface impingement jet, the fluids have a different nature (Molana & Banooni, 2013).

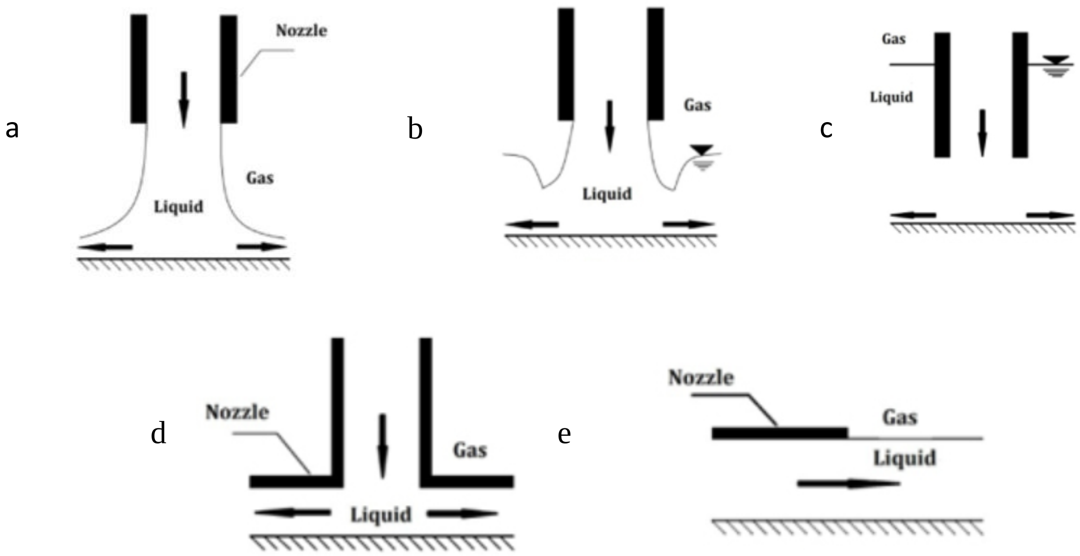

Figure 1.20 Types of impingement jets a) free surface b) plunging c) submerged d) confined e) wall (Molana & Banooni, 2013)

In this thesis, the effects of pressure, flow and distance to the heat transfer will be investigated. Experimental studies are performed on flat and concave surfaces. The results of the experiments on the flat plate are compared in the 3D analysis program.

CHAPTER TWO

EXPERIMENTAL SETUP AND MEASUREMENTS

Literature review and field research were conducted for the experimental study. Technical support was obtained from various companies for the design of the experimental setup. Many tests have been performed with the different types of cooling channels. Cooling pipe designs are changed because of the geometry of the wheel. Number, length and type of pipe system are affected the design of the wheel's spoke. To better understand the system, designs were made similar to the cooling system under production conditions and experiments were conducted.

Singh et al.(2013), used a schematic diagram of the experimental set up in Figure 2.1 Our system is very similar to Figure 2.1. In addition to the system, we also use digital manometer and flow meter (Singh, Premachandran & Kohli, 2013).

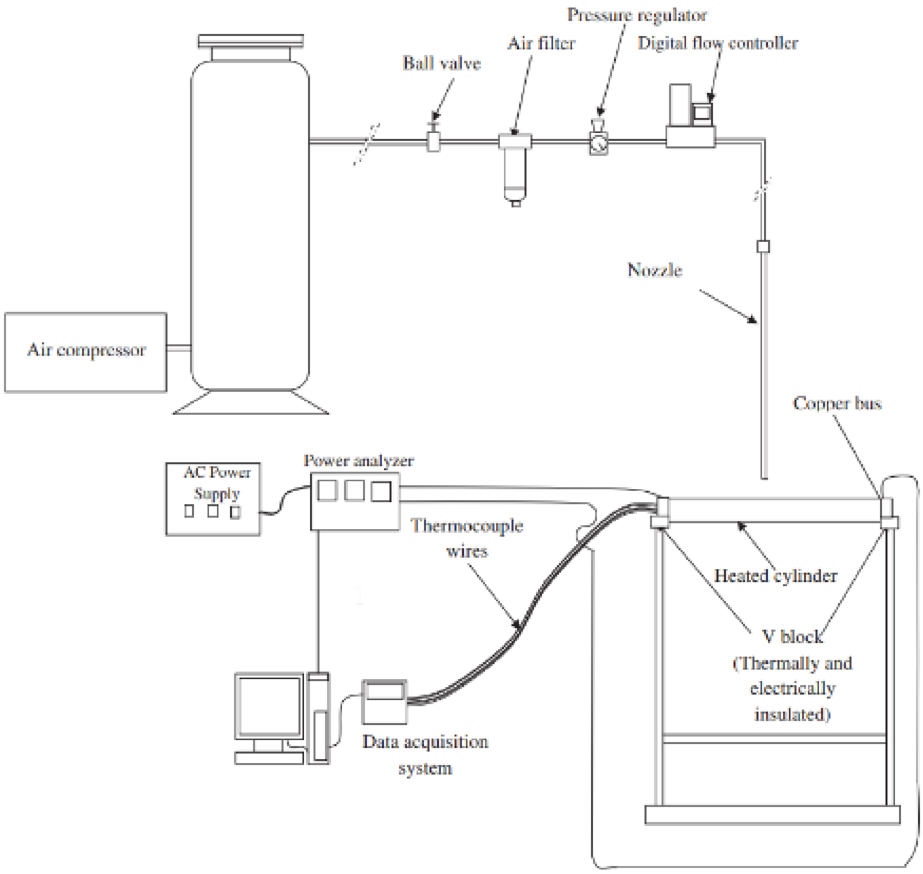

Figure 2.1 Schematic diagram of the experimental set-up (Singh, Premachandran & Kohli, 2013)

Our experimental system occurs;

1) Compressor system
2) Experimental system

2.1 Compressor System

The path of air in the compressor system is shown in Figure 2.1. The pressure of the system is maximum 6.5 bars. The reciprocating compressor delivers air to the air-tank which is used to prevent compressor failure and pressure fluctuations. Compressed air is transmitted to air filter for removing extraneous matter. And finally, air is transmitted to dryers where moisture in the air due to high pressure and temperature is removed.

Figure 2.2 shows the compressor system. The important points here are constant and dry air. Casting is adversely affected by pressure fluctuations. And the electronic devices which are used for monitoring pressure, flow, temperature, etc. are affected by moist air.

a

b

c

d

Figure 2.2 Cooling system a) compressor b) air tank c) filters d) dryer (Personal archive, 2019)

2.2 Experimental System

2.2.1 Cooling Pipe

Dried air was used in the experiments. Tests were performed with the cooling pipes shown in Figure 2.3. Some of these tests are heating-cooling process applied to different geometric surfaces and some of them are only experiments for measuring air consumption values. During flow, airflow characteristic is affected by the types and diameters of the pipes.

Experimental tests were carried out by different types of cooling pipes. In tests conducted with different pipes of the same type, it was observed that flow rates are affected by the burrs which occur in the pipe system. This is a major problem, especially for multiple nozzles. The closed nozzles cause some mold regions cools down late than the other regions. This may cause the internal structure to deteriorate in areas with late cooling.

a b c

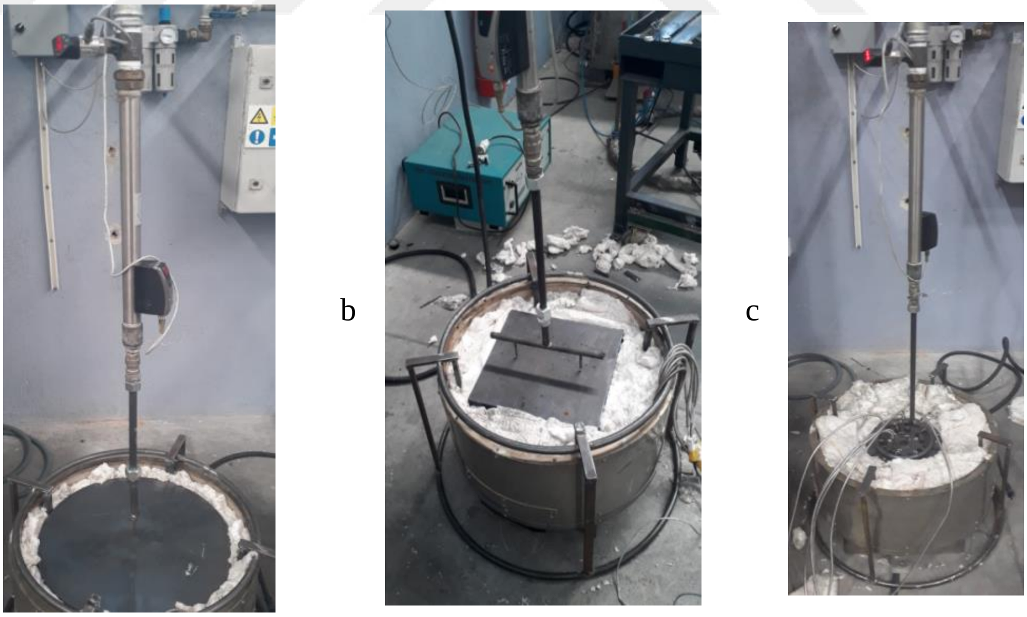

Figure 2.3 Nozzles a) single nozzle b) side block - two nozzle c) multi nozzles (Personal archive, 2019)

2.2.2 Thermocouples and Temperature Recording System

To record temperature K type thermocouple and Pico Tc-08 temperature recorder were used. Type K thermocouple is the most used type and described as Nickel-Chromium / Nickel-Alumel. This thermocouple has a wide temperature range and the maximum working temperature is 1200°C. Figure 2.4 shows the one single nozzle cooling system, circle mold and thermocouple locations. The 7 K-type thermocouples are located on an axial direction. Holes were drilled as possible as to mold surface close to observed the effect of the flow so M6 holes are drilled 2 mm to the surface. Thermocouples are attached to the mold by the connection parts.

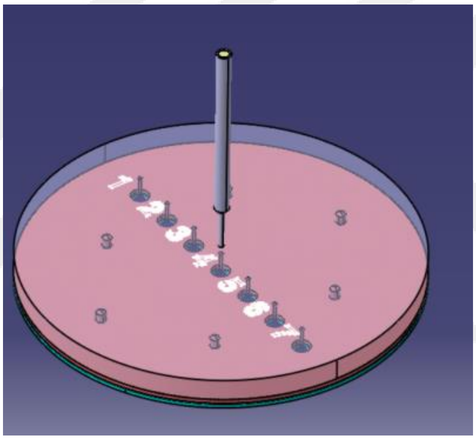

Figure 2.4 Thermocouple locations

Pico TC-08, PLW recorder software and K-type thermocouple are shown in Figure 2.5. The recording interval was 200 ms.

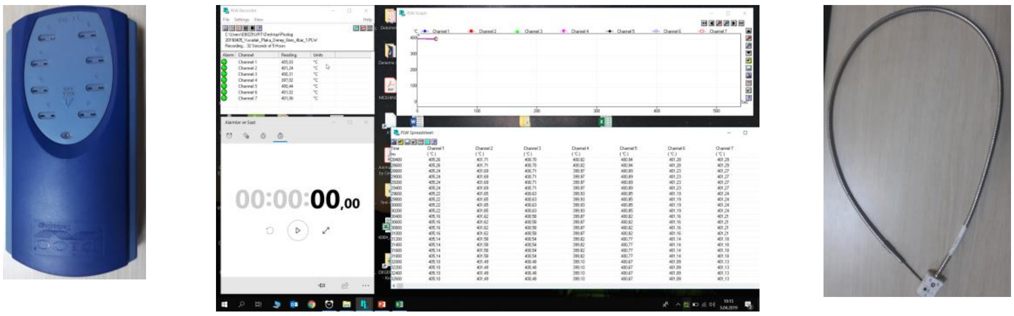

a b c

Figure 2.5 Datalogger, software and thermocouple (Personal archive, 2019)

2.2.3 Flow Meter

To measure the flow rate Testo 6442 was used. The Testo 6442 uses the thermal flow measurement method as the flow measurement principle in pressure lines. The sensor design and measuring principle are shown in Figure 2.6.

Figure 2.6 Measurement principle of flow-meter (Personal archive, 2019)

According to the thermal flow measurement principle, the air passing between two glass-coated ceramic sensors, one in contact with the sensor in the transmitter (at the temperature of the measuring medium) and the other in a controlled heating, changes the equilibrium state of the Wheatstone bridge circuit structure to which the sensors are connected.

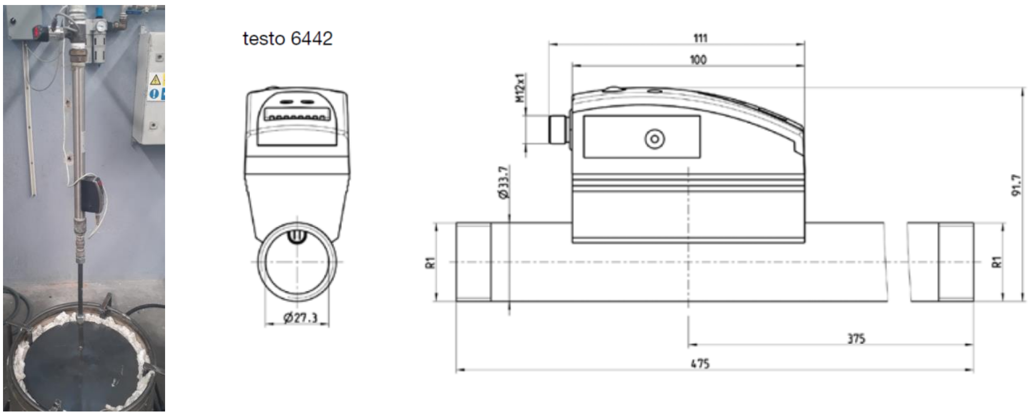

a b

Figure 2.7 Measurement principle of flow-meter (Personal archive, 2019)

In order to flow-meter to make accurate measurements, it is necessary to have a certain distance to the place of measurement. Therefore, the flow-meter has its own length and is shown in Figure 2.7

Testo 6442 flow-meter measures the flow rate by normalizing the volumetric flow rate in according to DIN ISO 2533 standards in order to achieve comparable measurement results on lines with different pressure values. Therefore, the unit is given as Nm^3/h for flow measurement and the unit is Nm^3 for consumption measurement. DIN ISO 2533 accepts the conditions of the measuring environment as 15ºC temperature, 1013 hPa (1 bar) pressure and 0% RH humidity. Accordingly, the following formula can be used to change from the flow-rate/consumption value given in the standard measuring conditions to the flow-rate/consumption value under operating conditions:

$$V_P = V_N (P_N/P_P) (T_P/T_N) \tag{2.1}$$

In this equation, V_N is normalized flow rate according to DIN ISO 2533 (output from the device, (Nm^3/h)), V_P is flow-rate under operating conditions (m^3/h), P_N is pressure value according to DIN ISO 2533 (1 bar), P_P is pressure value under operating conditions (pressure of your line), T_N is temperature value in (K) according to DIN ISO 2533 (15ºC = 273+15 = 288K), T_P is temperature value under operating conditions. (Line temperature. If not specified, ambient temperature)

2.2.4 Digital Manometer

During the first period of the test, pressure had been read from the regulator mechanic indicator. However, it was observed that mechanical manometer deviated from some values, so tests were carried out with the digital manometer.

WIKA PSD-30 pressure transmitter was used for the reading system, is shown Figure 2.8 WIKA accuracy is 0.5% and could measure between 0-10 bars.

Figure 2.8 Digital manometer (Personal archive, 2019)

Another important issue in pipe system works is the pressure occurring in the pipe. Differences between total, static and dynamic pressures are important in some systems.

$$P_{Total} = P_{Static} + P_{Dynamic} \tag{2.2}$$

In this equation, P_{Total} is measured by Pitot tube, shown in Figure 2.9 (bar) and sum of the P_{Static} and $P_{Dynamic}$. P_{Static} is the pressure of the fluid in the pipe at rest (bar). $P_{Dynamic}$ is the dynamic pressure volumic kinetic energy of the fluid ($P_{dynamic}=1/2\rho V^2$, bar)

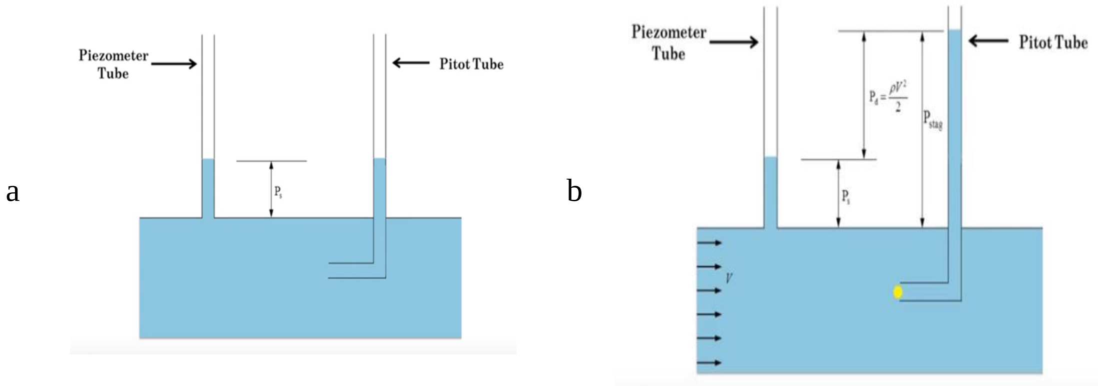

Figure 2.9 Pressures a) static pressure b) total pressure

2.2.5 Heating System

Protherm device is used to heat the system. Power is 3600W, voltage is 220V, current is 16I(max), frequency is 50/60 Hz. Figure 2.10 shows Protherm Device, Figure 2.3 shows the apparatus for heating the upper mold offset and Figure 2.3.c shows the isolated surfaces. Figure 2.10 shows the general view of the test system.

a  b 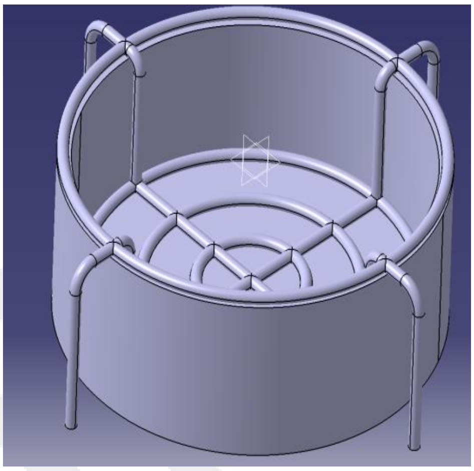

Figure 2.10 Heater a) protherm heater b) constructive design (Personal archive, 2019)

The constructive design was prepared to prevent the surfaces and the thermocouples to be damaged from resistances of the Protherm. Materials to be tested are placed on this design. There is a distance between the test material side surfaces to be tested and the inner diameter of the Protherm. Thermocouples are taken out from here. This surface is insulated with fiber material. Figure 2.11 shows the flat test material, data logger, insulation materials and exit of thermocouples.

Figure 2.11 Thermocouples and insulation materials (Personal archive, 2019)

In mathematical and numerical calculations, the bottom and side of the test surfaces were taken adiabatic. Many test systems had been observed for isolations. Experimental systems were observed by the thermal camera for isolation control. Finally, Protherm heater system was dedicated to use. Figure 2.12 shows the different contrast of the test system with the thermal camera. Especially Figure 2.12.c shows when the thermal camera is adjusted the minimum temperature of the 100°C. The system is therefore suitable.

a) b) c)

Figure 2.12 Isolation control of test system with thermal camera (Personal archive, 2019)

2.3 Experimental Test Results

For understanding the behavior of the air cooling system, there had been made lots of tests. In this section, some of them are given with detail. Tests were carried out with a single nozzle, side block - Two nozzle and multi nozzles which showed in Figure 2.3.

2.3.1 Single Nozzle Test Results

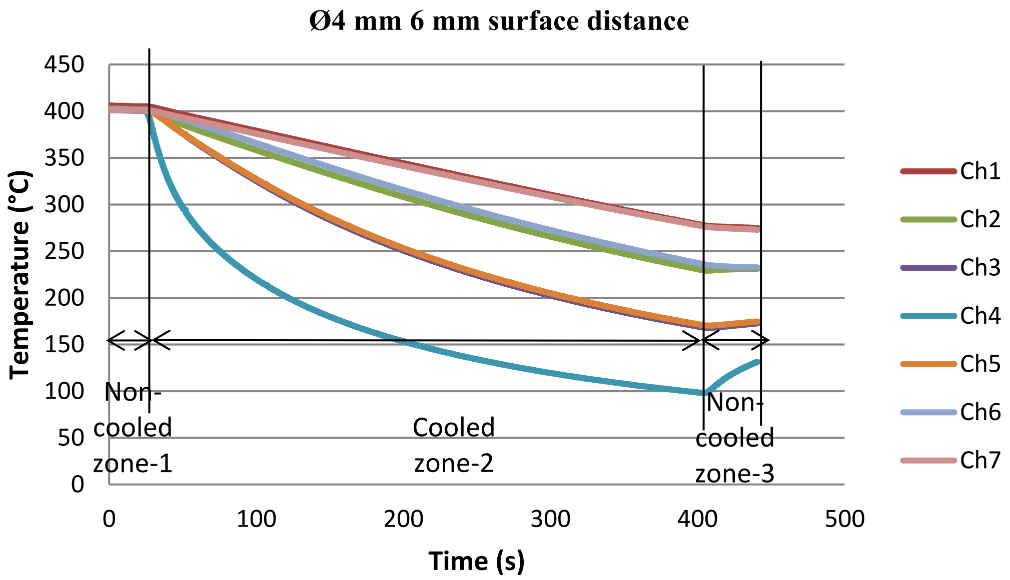

Figure 2.13 Single nozzle Ø4 mm surface distance 6mm

In Figure 2.13 single nozzle test result is shown. System pressure was 4 bars and distance between surfaces was 6 mm. The figure is separated into 3 zones as non-cooled zone-1, cooled zone-2 and non-cooled zone-3. The first zone is called non-cooled-1period which system was heated until 401°C and turned off, the temperature of mold reached 408°C by the inside of the Protherm heat and then temperature decreased 100°C with environment temperature.

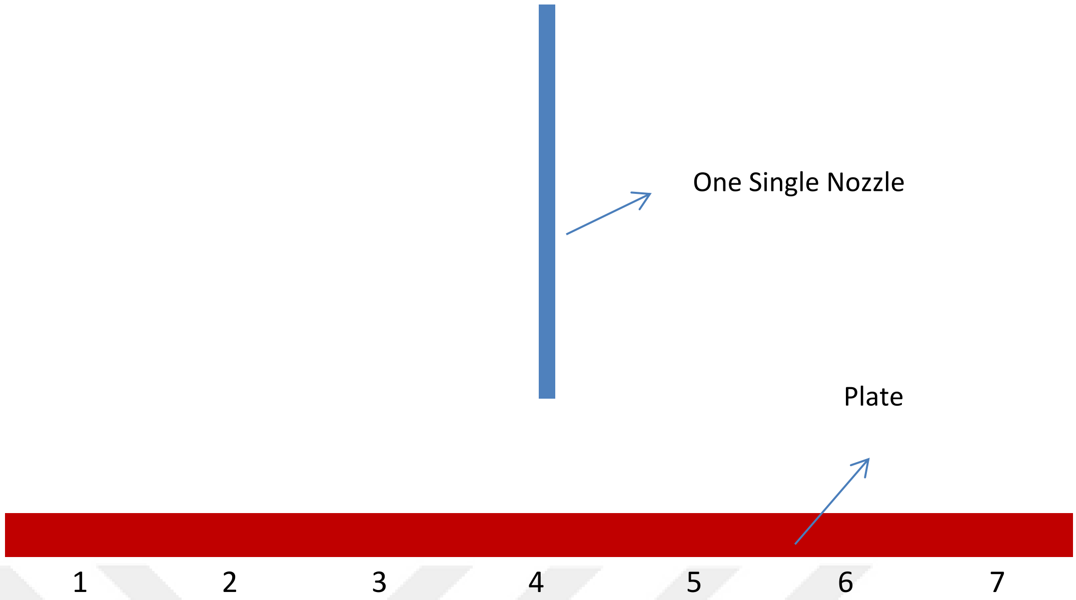

Figure 2.14 One-single nozzle and thermocouples locations

The flat mold was used for the single nozzle system and radius of flat mold was 215 mm. In Figure 2.14, 7 thermocouples, the nozzle and the flat mold were shown as 2D. As mentioned above, Channel 4 was used for temperature control from a point due to the necessary reference.

Table 2.1 Temperature of the points at the different zones

		Ch1 °C	Ch2 °C	Ch3 °C	Ch4 °C	Ch5 °C	Ch6 °C	Ch7 °C
Non-cooled zone 1	**Turn-off the heater**	404.05	403.25	405.25	401	400.25	402.65	403.25
	The highest temp	408.65	407.5	409.25	408.25	407.65	408.75	408.65
Cooled Zone	**Cooling start**	401.25	401	400.5	400.75	400.65	401.25	400.65
	End of the test	281.47	233.41	171.71	100.04	172.09	235.16	280.16

Distributions of temperatures at different thermocouples are shown in Table 2.1. As shown in Figure 2.14, Ch1-Ch7, Ch2-Ch6, Ch3-Ch5 are symmetry and Ch4 is for a single temperature. For symmetry thermocouples, the temperature values should be close to each other. Table 2.1, first column (Turn-off the heater) shows the differences in temperature for symmetrical thermocouples. The system was shut down when the ch4 was at 401°C. In column 2, the temperature of Ch4 reached a maximum of 408 degrees. After this point, the temperature began to decrease. When Ch4 decreased 400 degrees, other temperatures were observed to be close to each other and the cooling system was switched on. Then the second zone, cooled zone continued until the Ch4 decreased the 100°C. Then, when Ch4 decreased to 100°C, symmetrical thermocouple temperatures were checked. In Table 2.1, the fourth column shows the test results. The temperature distributions were observed to be symmetrical. Until this result had reached, many tests had been carried out. On the other, to accurate our test, many tests had been carried out the same conditions (at the same distance and bar).

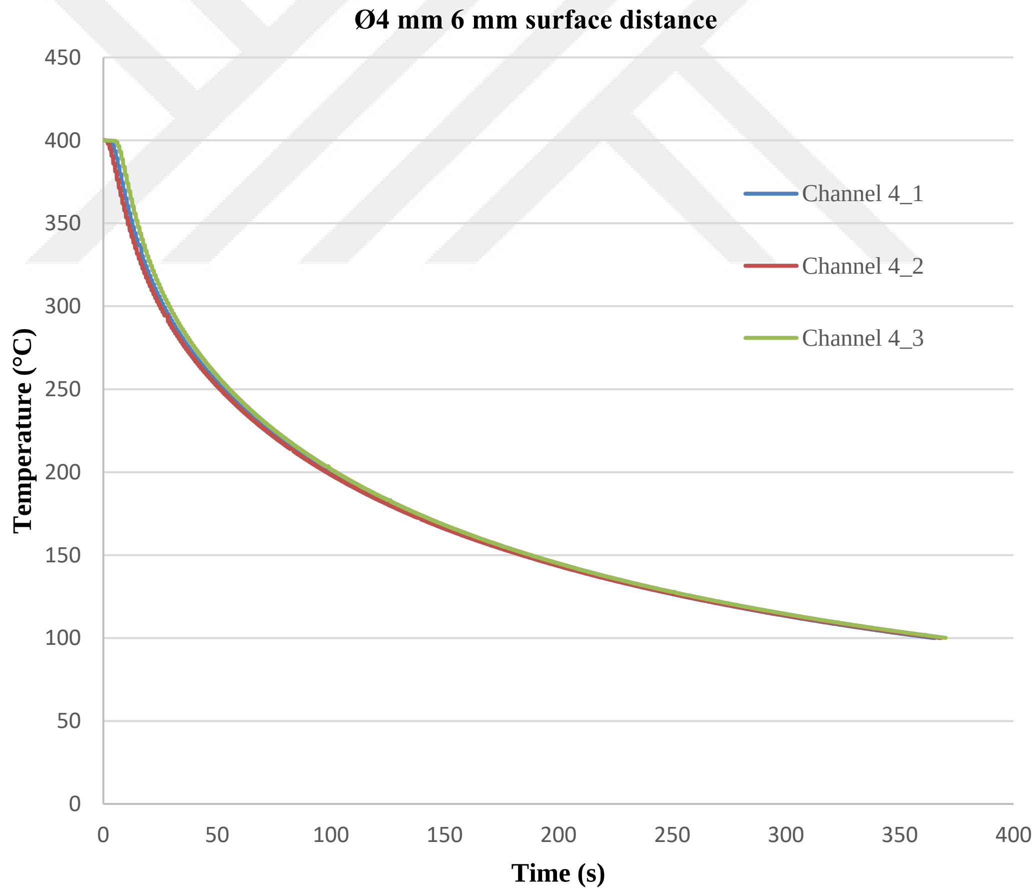

Figure 2.15 Test validation trials

Figure 2.15 shows the Channel 4 test results which were carried out with Ø4 mm nozzle diameter, 6 mm distances between surface and nozzle and at 4 bars pressure. These tests were repeated 3 times with the same conditions. The test results overlap as shown in Figure 2.15 The tests were started at 400°C and completed at 100°C. The times of tests were 6 min 5 s, 6 min 5s and 6 min 1s, respectively. In this way, the tests were verified.

Table 2.2 Test result at different pressure (Ø4 mm Nozzle, 6 mm surface distance)

Surface Distance	6	6	6	6	6
Bar	3	3.5	4	4.5	5
Flow (Nm^3/h)	28	33	37	42	46
Ambient Temperature	20°C	20°C	20°C	20°C	20°C
Time	07 min 17 s	6 min 34 s	6 min 5 s	5 min 37 s	5 min 27 s
Heated Temp (Ch4)	401°C	401°C	401°C	401°C	401°C
End of Test (Ch4)	100°C	100°C	100°C	100°C	100°C

The flow changes with pressure are shown in Figure 2.16. The flow-rate increases with linear with pressure. As the flow-rate increases, the amount of air moving to the surface of the mold will increase. This flow will increase the heat transfer and the mold cool faster.

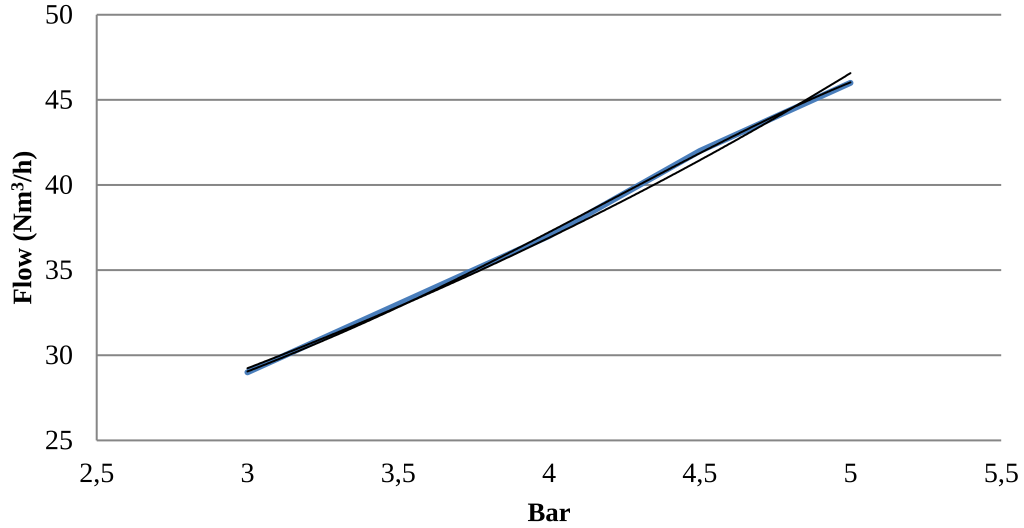

Figure 2.16 Interaction between the pressure and flow-rate

Temperature-time changes are shown in Figure 2.17. Internal structure defects that may occur during casting can be eliminated at different flow rates. However, another important issue is the calculation of energy consumption. Compressed air production is very costly. For this reason, the cooling system must be operated optimally.

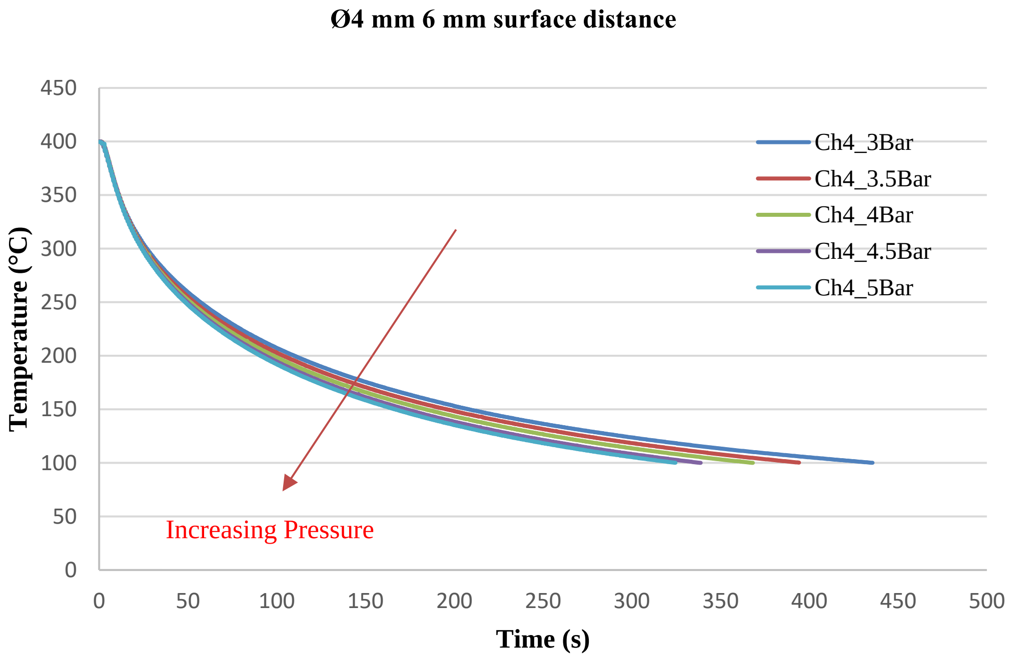

Figure 2.17 Temperature-time changes Ø4 mm and at 6 mm distances

These experiments were carried out distances between mold surface-nozzle to be 2,4,6,8 and 10, respectively. Table 2.2, Figure 2.16 and 2.17 show the Ø4 mm nozzle, 6 mm surface distance and different pressures. The other test results are detailed in Figure 2.18 which represents temperature-time changes at different distances and pressures. In section 2.1 is detailed that the compressor system produces maximum 6.5 bars. If the figures (2.17 and 2.18) are examined in detail, after the 4.5 bar some problems may have been occurred because of the pressure fluctuation. In the mold facilities, there are many machines work with air. So the pressure fluctuation may have occurred when the experiments were carried out with the other machines. Also, these situations may occur, when the serial productions. Therefore, this must also be taken into account in serial production.

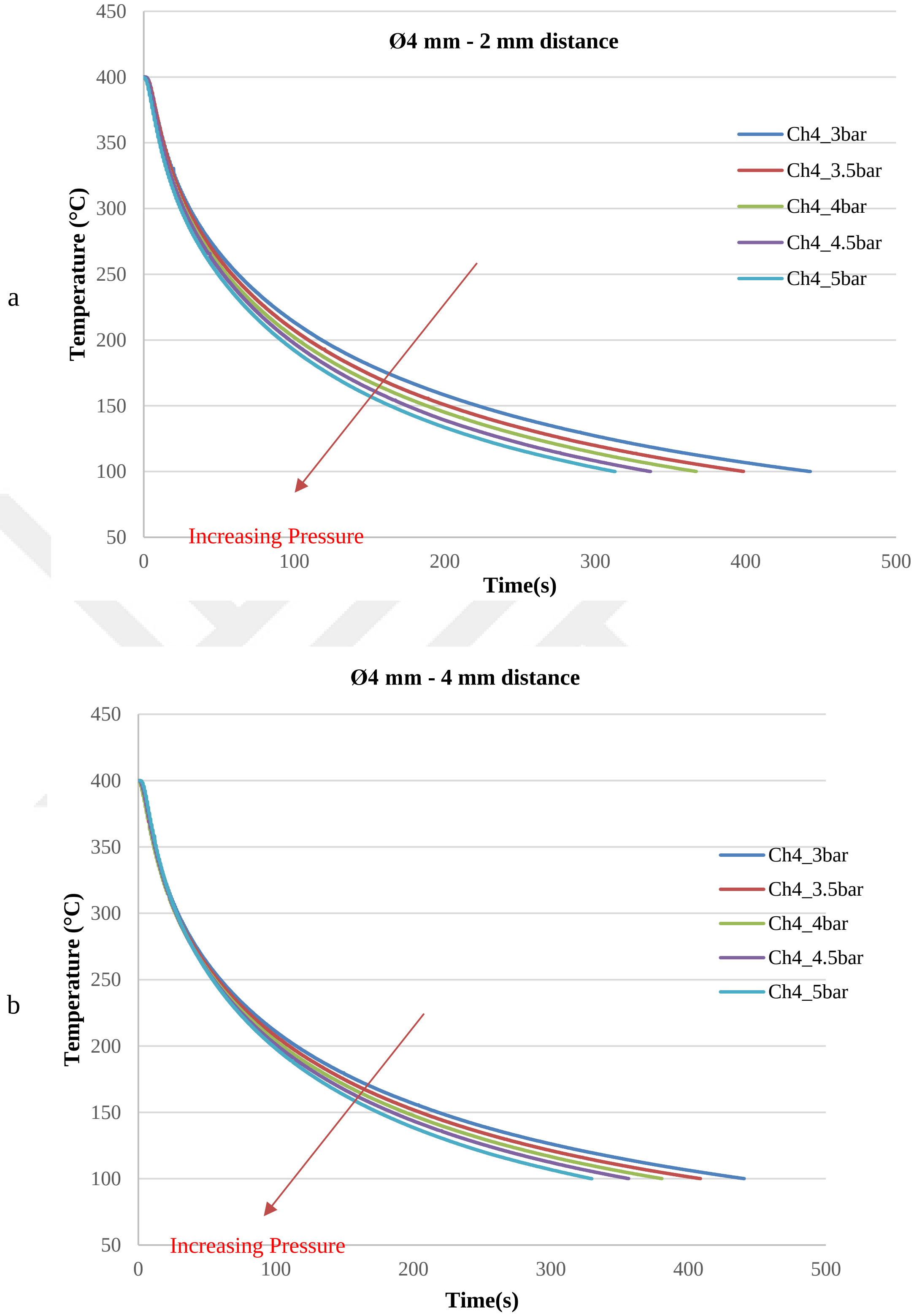

Figure 2.18 Temperature-time changes at different distances and pressures

c

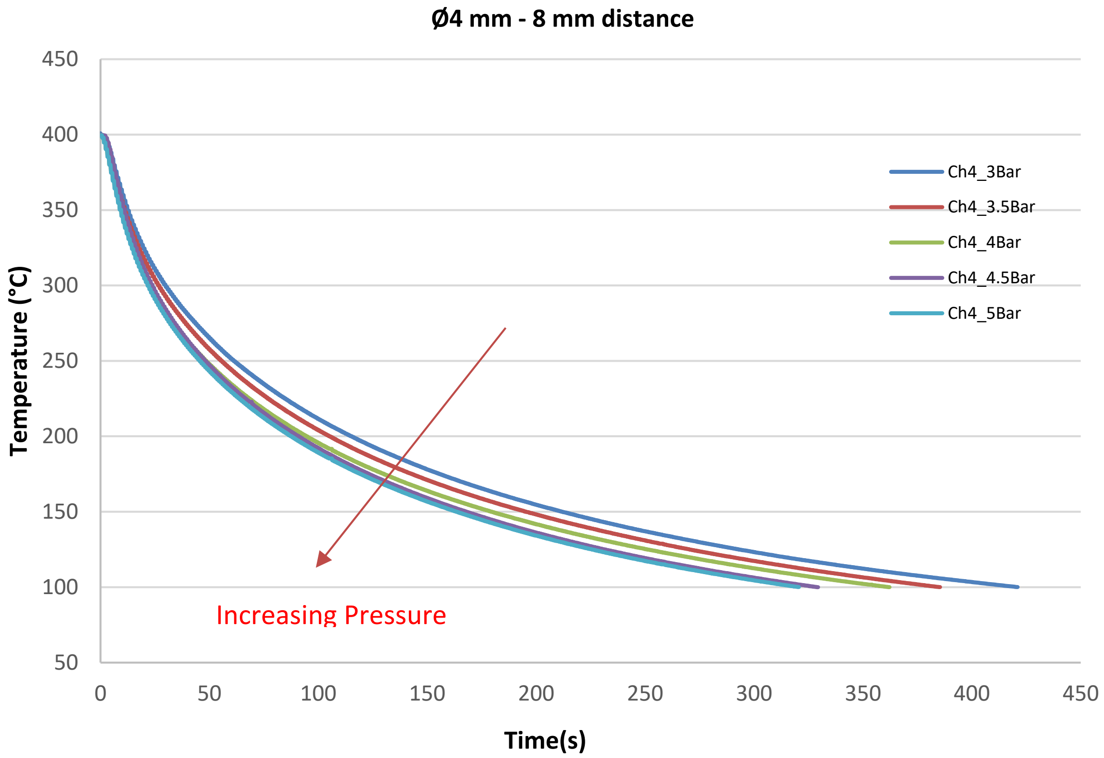

d

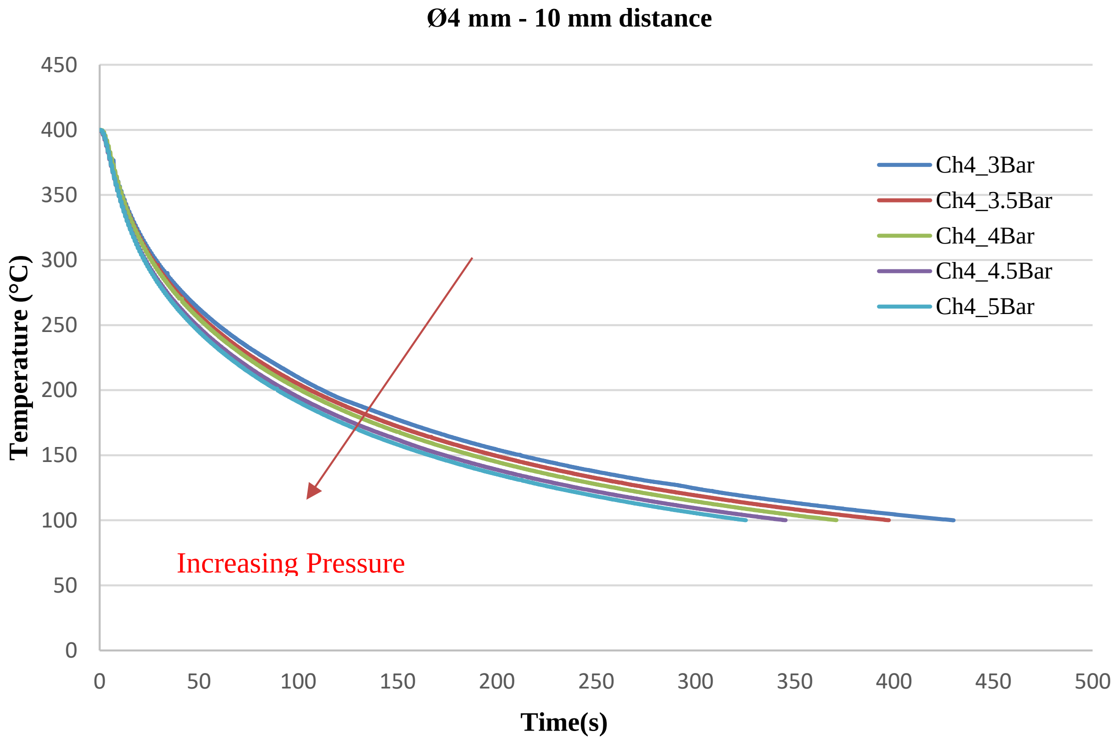

Figure 2.18 continues

The Nu and h values of the experimental results of the study, which has a numerical study diameter Ø4 mm and a surface distance 6 mm, were calculated.

The following equation was used for the heat transfer coefficient to be obtained depending on time. (Akçay , 2011)

$$m_i c_{pi} \frac{dT_i}{dt} = h_i A_i (T_{si} - T_j) + \varepsilon \sigma A_i (T^4{}_{si} - T^4{}_c) \tag{2.3}$$

In this equation m_i is the mass of flat plate (kg), A_i is the surface of flat plate (m^2), T_j is outlet air temperature of nozzle (293.15K), ε is radiation emission rate of flat plate (for 1.2344, hot-tool-steel ε=0.7), σ is constant of Stefan-Boltzman $5.67x10^{-8} Wm^{-2}K^{-4}$, T_{si} is temperature of flat plate, T_c is surrounding temperature, c_{pi} is the specific heat value for the every each surface temperature, ρ is the density of flat plate (7367 kg/m^3).

Heat transfer coefficients are calculated for the 3, 4, and 5 bars by Equation 2.3 and represented in Figure 2.19-20-21.

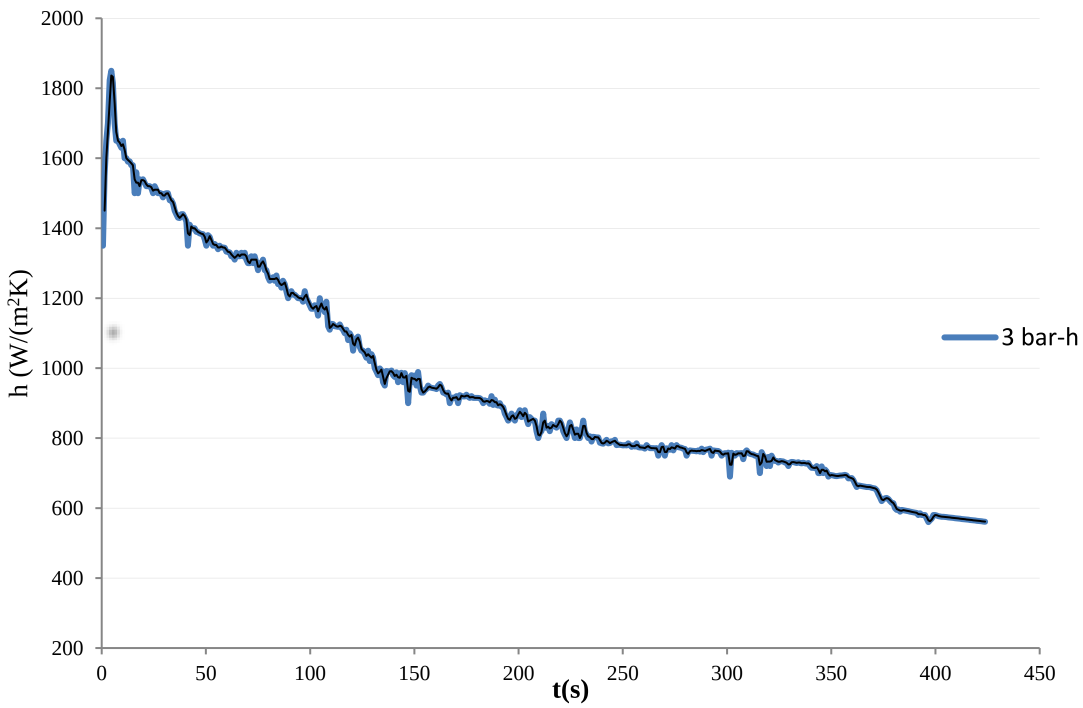

Figure 2.19 Average heat transfer coefficient for 3 bar

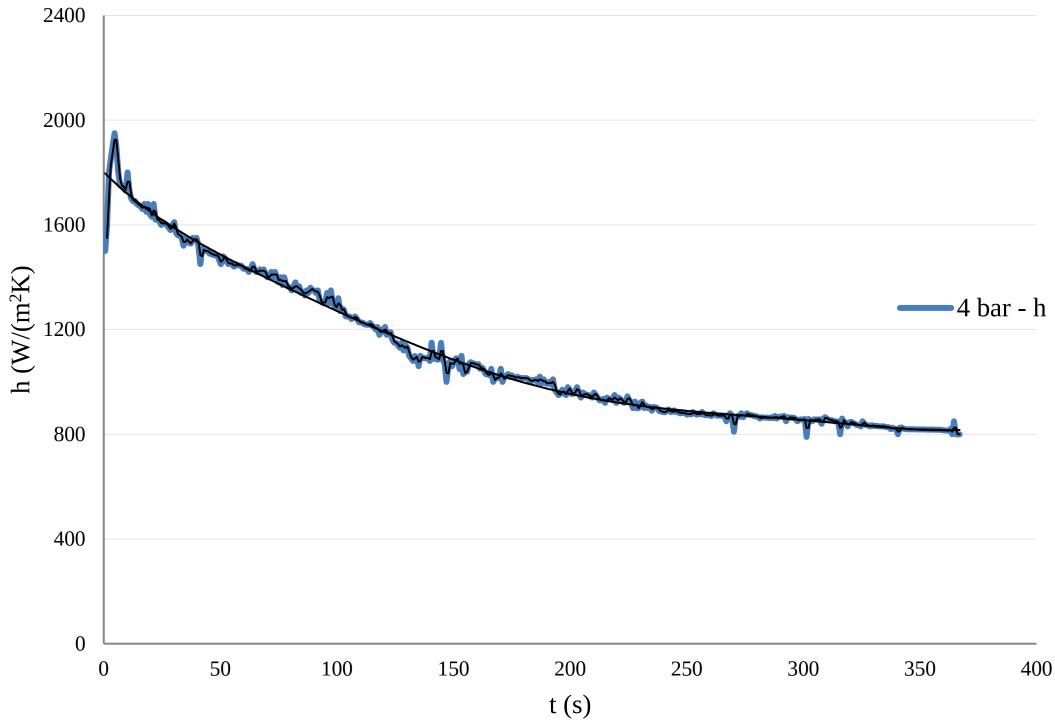

Figure 2.20 Average heat transfer coefficient for 4 bar

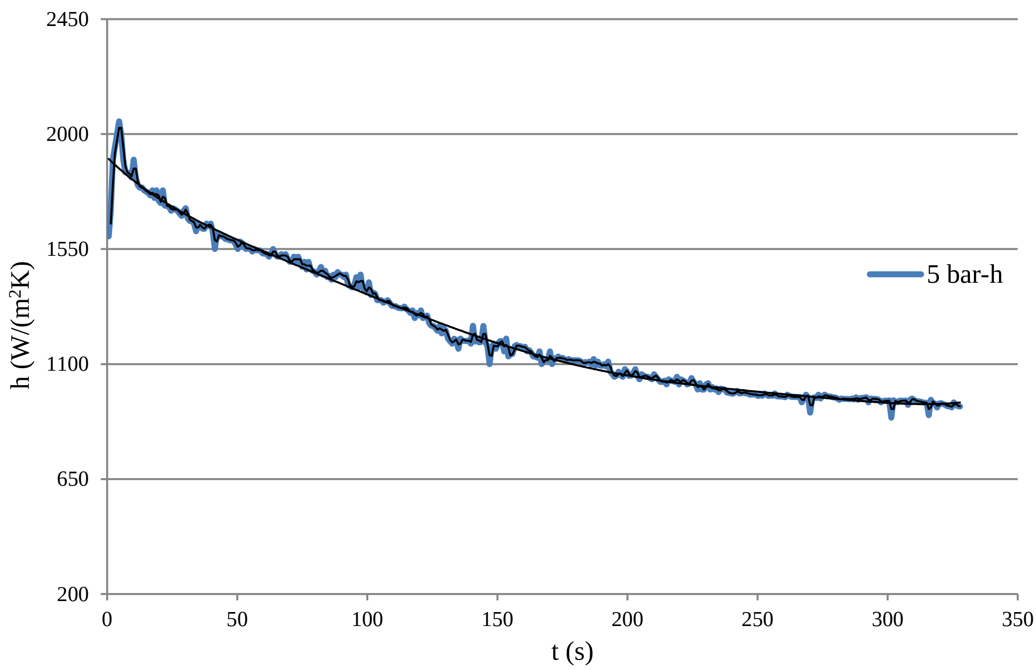

Figure 2.21 Average heat transfer coefficient for 5 bar

Nusselt numbers are calculated by Equation 1.5. In convection studies, it provides a measure of the convection heat transfer at the surface. In Figure 2.22 shows the average Nusselt number for the 3, 4 and 5 bars depending on time.

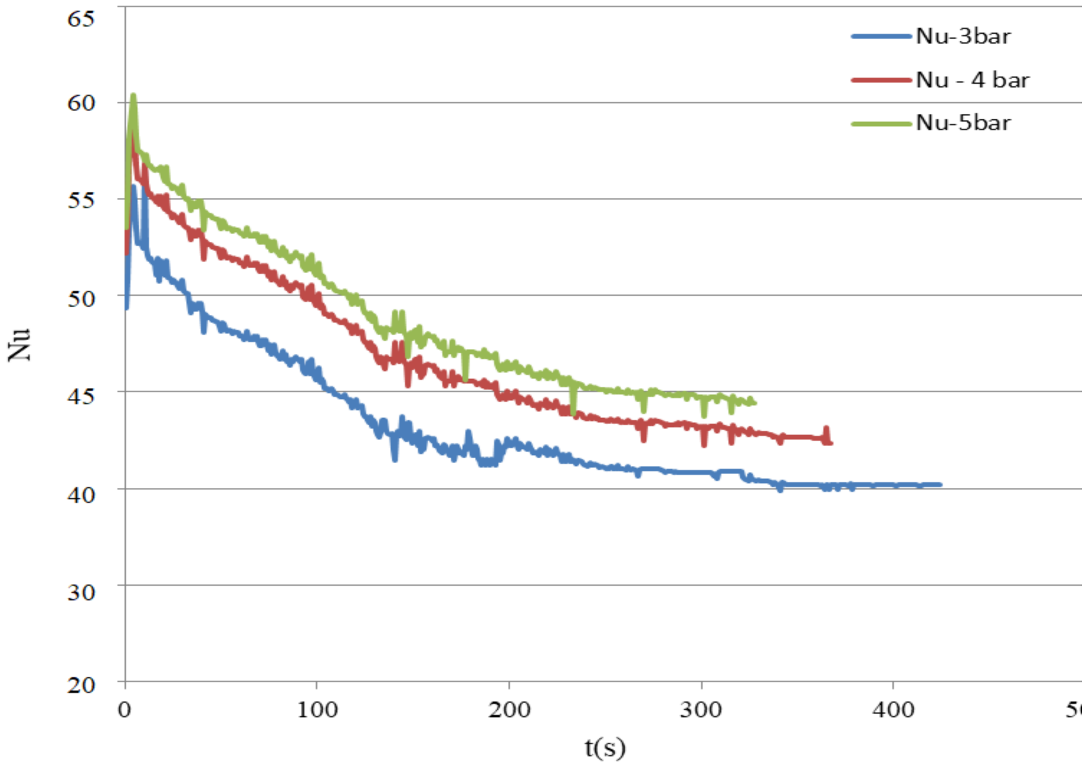

Figure 2.22 Average Nusselt number

2.3.2 Multi Nozzle Test Results

In this section, upper offset mold will be examined. This region of the mold was raised to a certain temperature and then cooled by different nozzle cooling pipe. Nozzle numbers and variety are changed according to the number of bolts. In this study number of nozzles are 5 and angles are 72°. So, 5 thermocouples were used. Thermocouples were located near the nozzles.

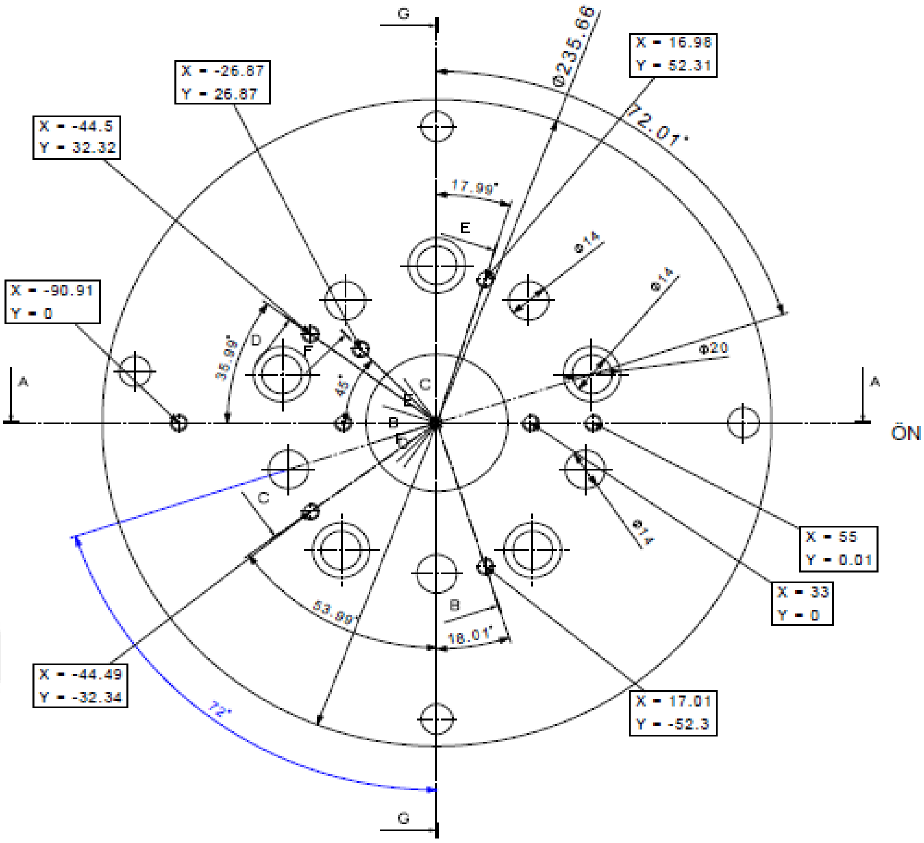

Figure 2.23 Two-dimensional drawing of thermocouples location

In Figure 2.23 thermocouples and cooling holes are shown as 2D. Unlike the previous section, there is a nozzle for each thermocouple. However, the fourth thermocouple was chosen as the reference, because of the difficulties of the cooling system control. The deviation of temperatures was observed almost ±5°C. As in the previous section, many tests had been carried out to ensure the best distribution of temperatures. Different tests were performed at the temperatures to be tested. For upper offset mold, the system was heated 501°C and then energy was turned off. Our furnace was absorbing the heat, so when the thermocouple 4 showed 501°C, the energy was turned off. The temperature of mold increased to the specific heat, almost 508°C. After that, the temperature decreased slowly to 500°C. When the thermocouple 4 showed 500°C, the cooling system was activated.

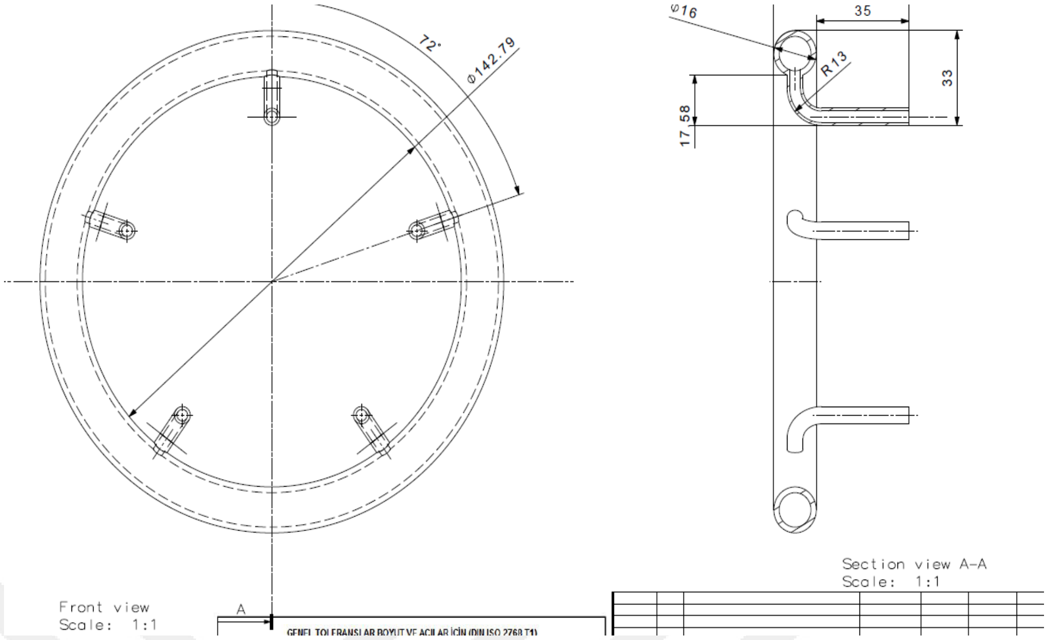

Figure 2.24 Two-Dimensional drawing of pipe

In Figure 2.24 and 2.25 show the cooling pipe. 2 and 4 mm diameter of pipes were used for the pipe system. The effects of the diameter of nozzle and distance of the surface to the cooling system were investigated.

a)

b)

Figure 2.25 Ø2 and Ø4 mm nozzles (Personal archive, 2019)

The investigations were carried out at 3, 3.5, 4, 4.5 and 5 pressures with Ø2 and Ø4 mm diameter pipes. And Figure 2.26 shows the change of pressure and flow rate with Ø2 and Ø4 mm diameter pipes. With the change in diameter, the flow has changed drastically. And also flow-rate affected the cooling time.

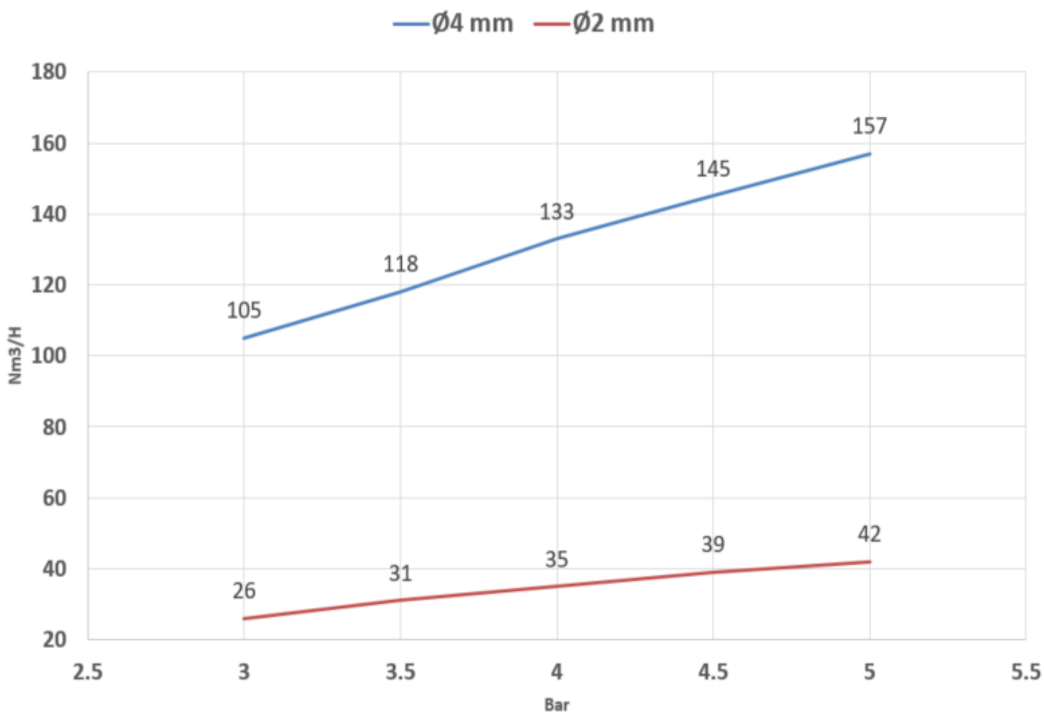

Figure 2.26 Change of pressure and flow-rate

The tests were also repeated 2-3 times, in order to verify the study. As the explained previous section, the 4th channel was accepted the reference channel throughout the study.

2.3.2.1 Ø4 mm Nozzle Study

In Figure 2.27 shows the experimental study with nozzle diameter Ø4 mm, surface distance 2 mm and system pressure 3-bar. Flow-rate was measured 105 Nm^3/h. When the variations of temperatures were examined, temperature distributions were observed to be fine. The cooling system was started when channel 4 was 500°C and the system was closed when it reached 300°C. And Figure 2.28 shows the test results at different pressures and distances with Ø4 mm nozzle. As the pressure was increased, the flow rate through the pipe increased. Temperature was reduced faster by increased flow rate.

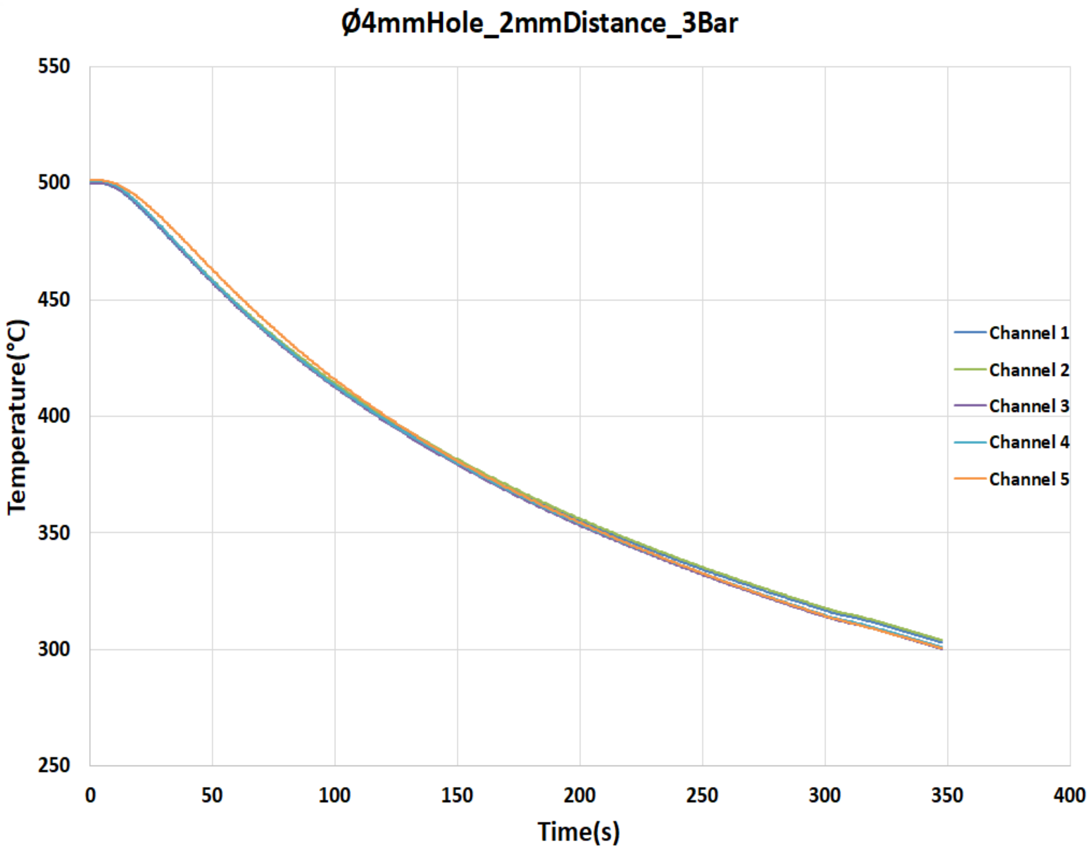

Figure 2.27 Ø4 mm nozzle, 2 mm distance, 3 bar

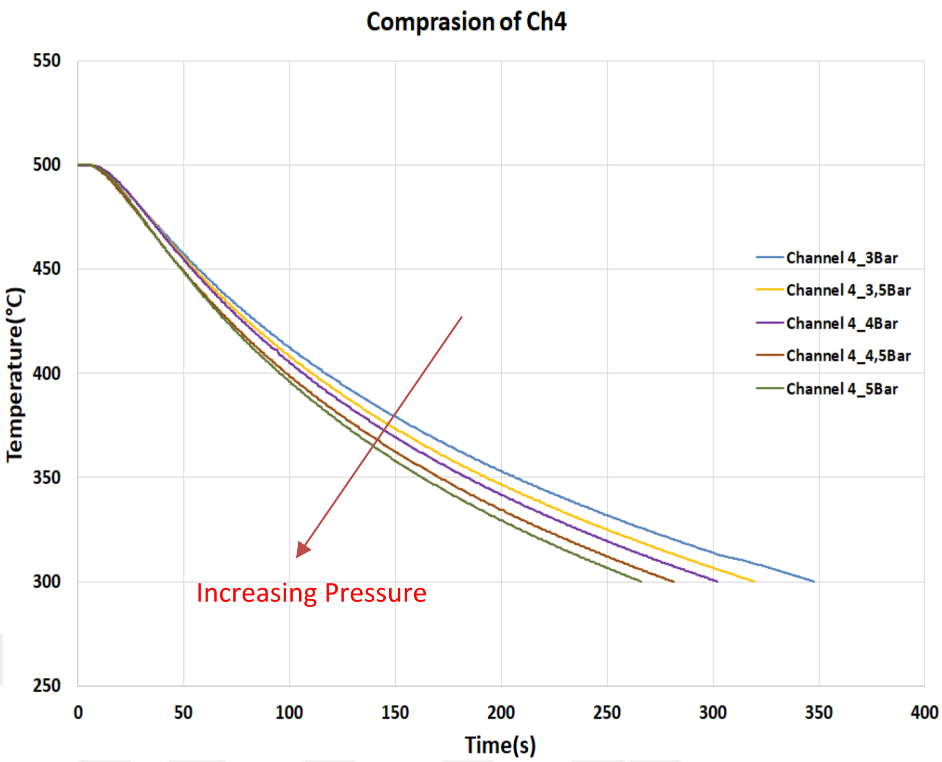

2 mm distance at different pressure (Ø4)

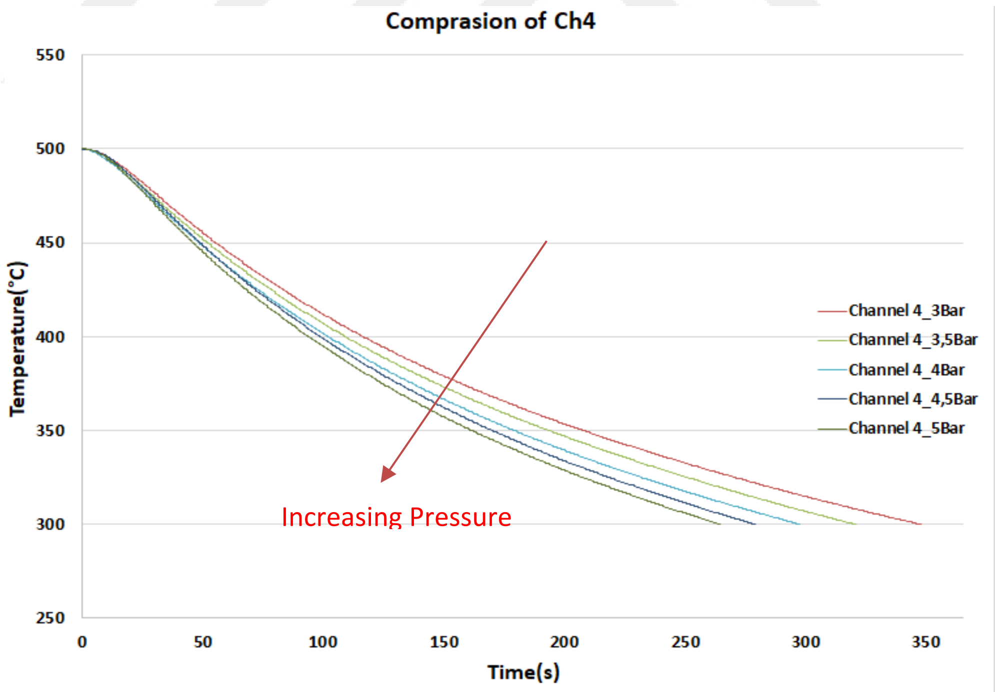

4 mm distance at different pressure (Ø4)

Figure 2.28 Test results at different pressures and distances with Ø4 mm nozzle

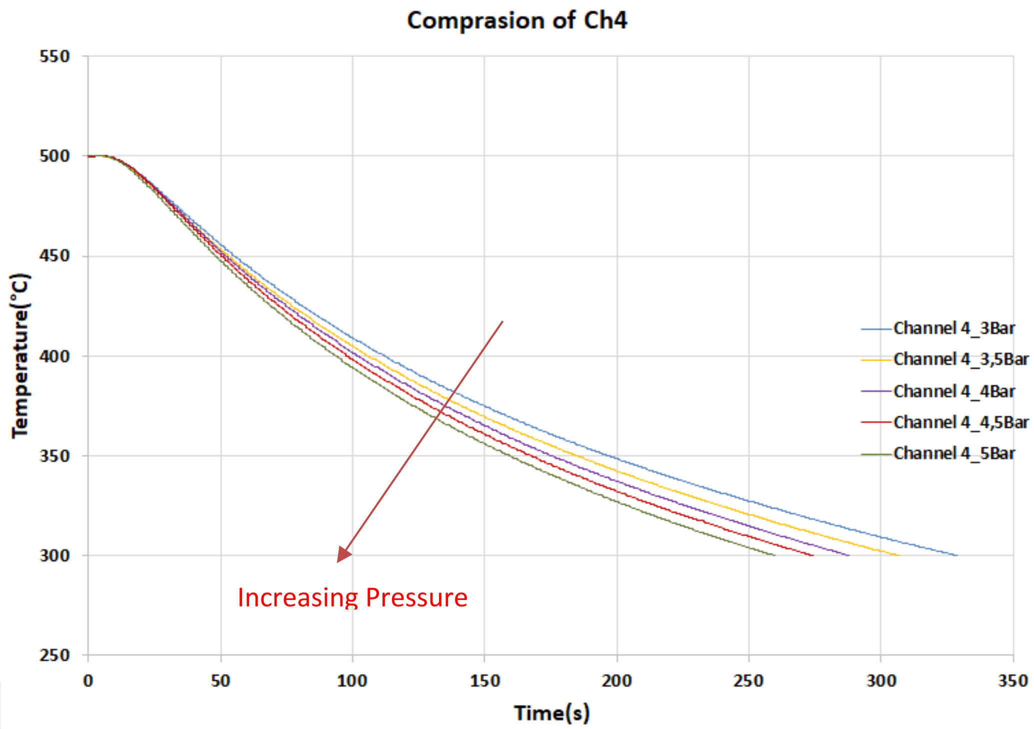

6 mm distance at different pressure (Ø4)

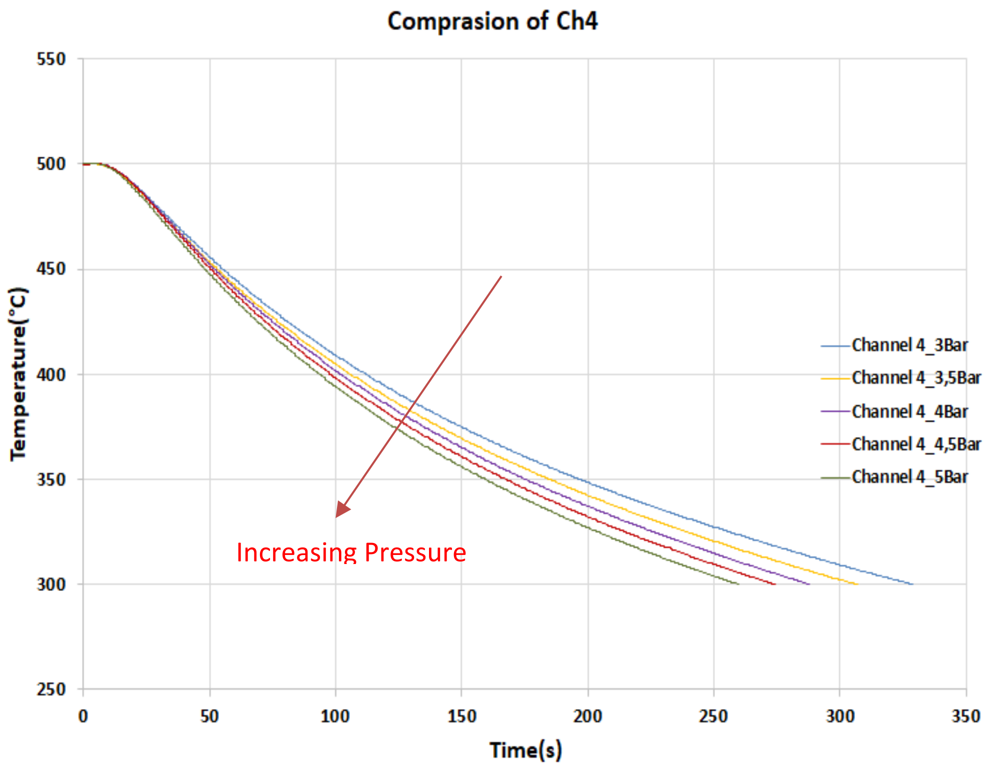

8 mm distance at different pressure (Ø4)

Figure 2.28 continues

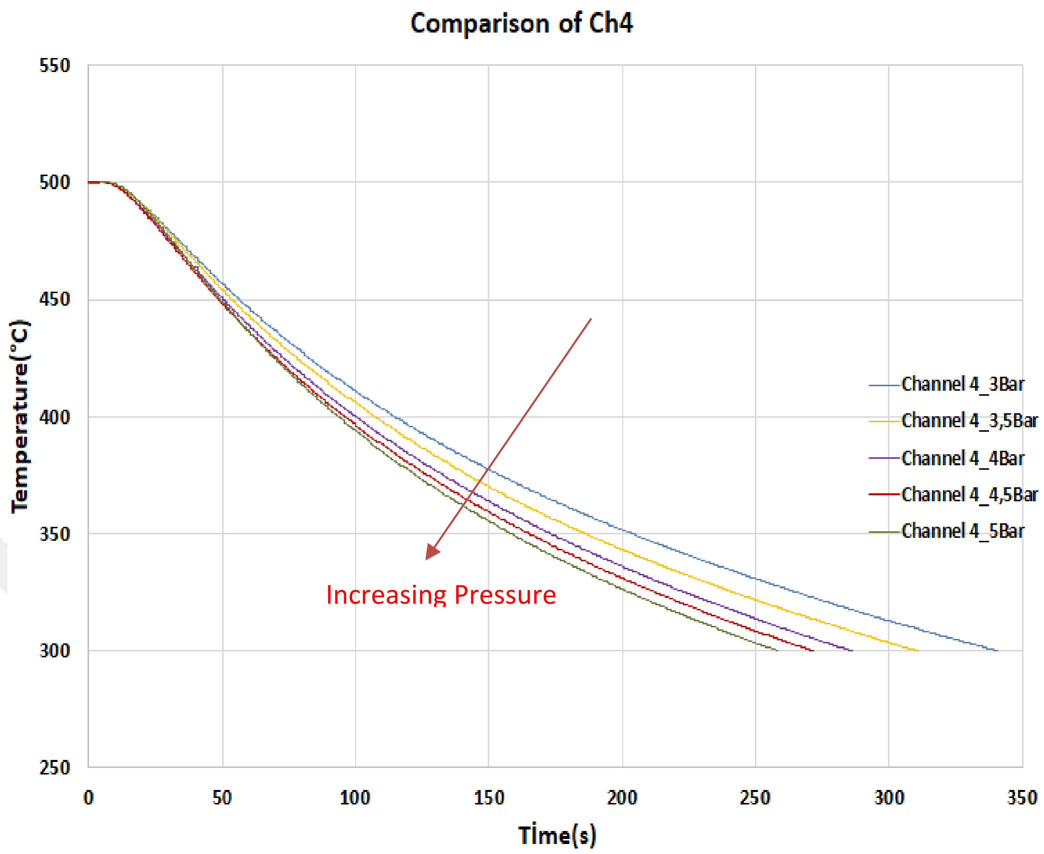

10 mm distance at different pressure (Ø4)

Figure 2.28 continues

2.3.2.2. Ø2 mm Nozzle Study

Figure 2.29 shows the test results at different pressures and distances with Ø2 mm nozzle. The same state was observed here as with in Ø4 mm diameter. As the pressure was increased, the flow rate through the pipe increased. Temperature was reduced faster by increased flow rate.

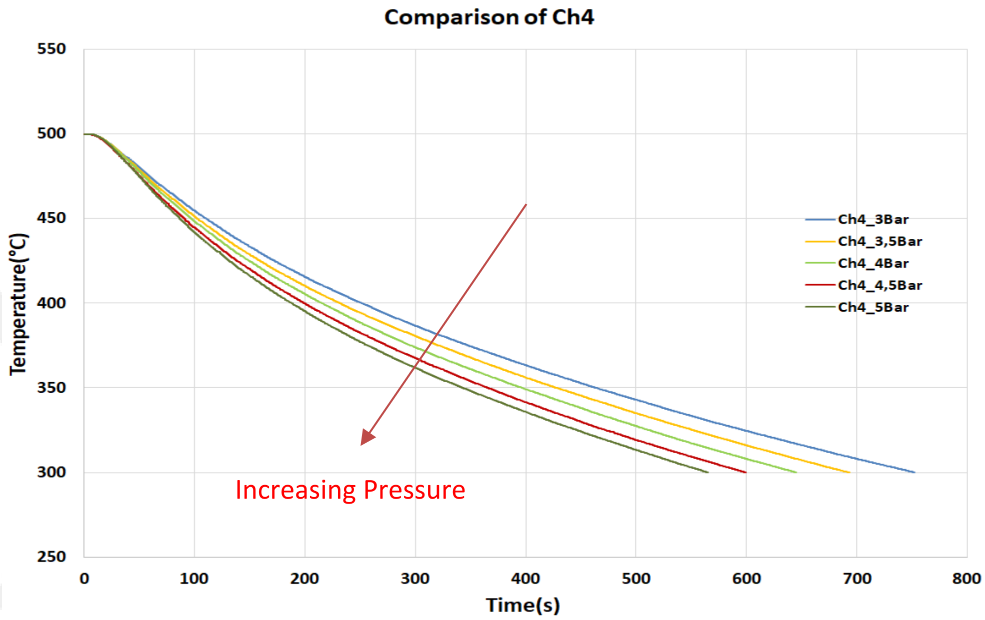

2mm distance at different pressure (Ø2)

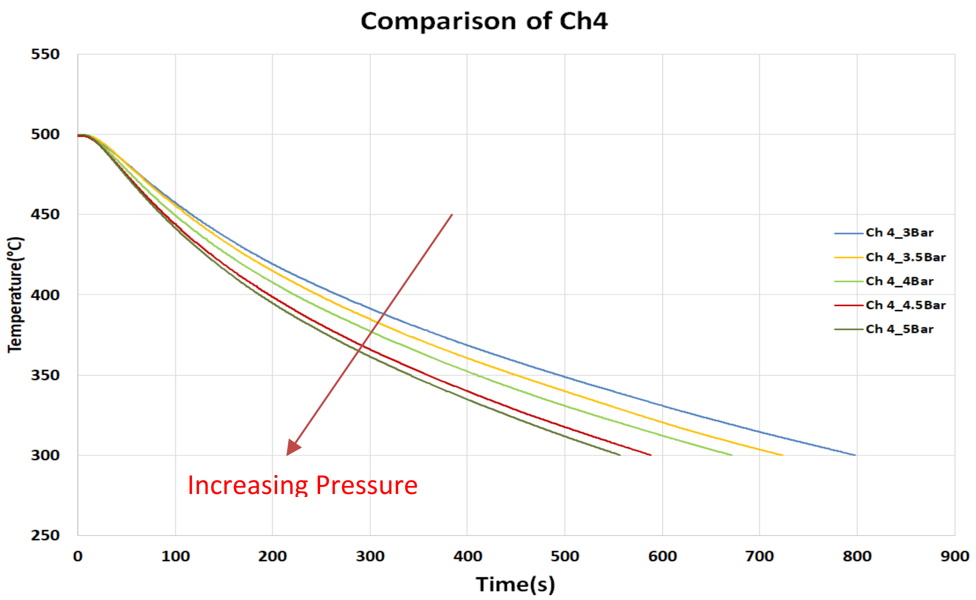

4mm distance at different pressure (Ø2)

Figure 2.29 Test results at different pressures and distances with Ø4 mm nozzle

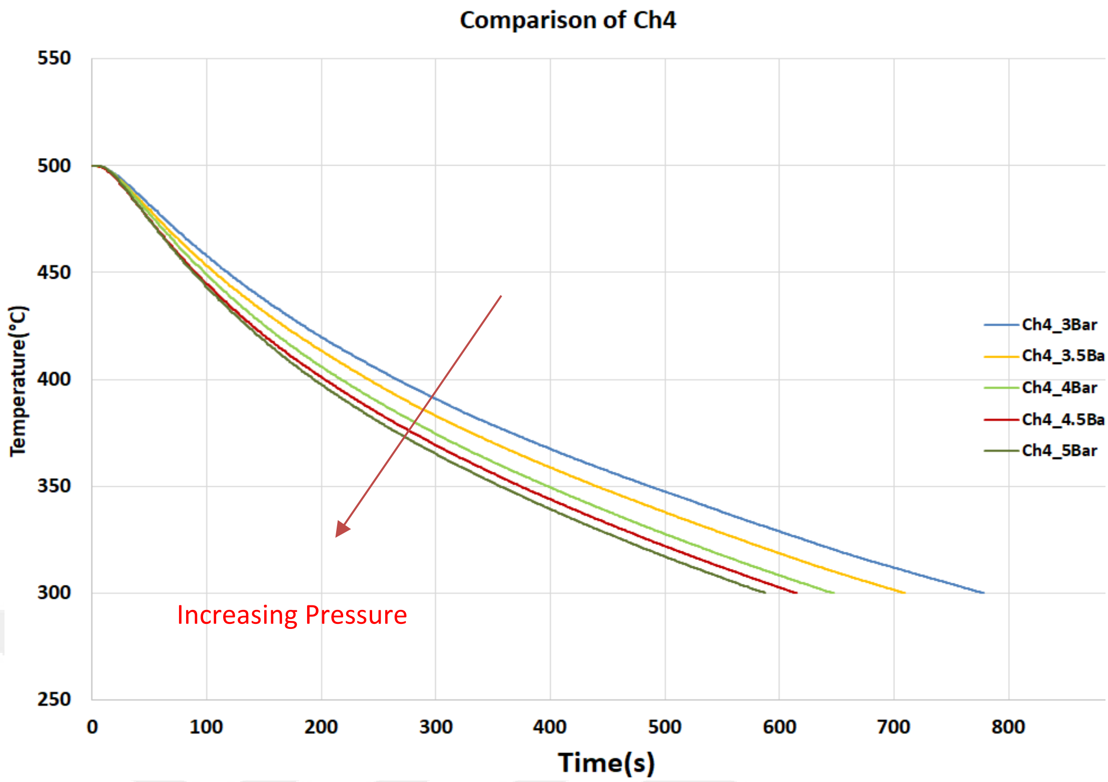

6mm distance at different pressure (Ø2)

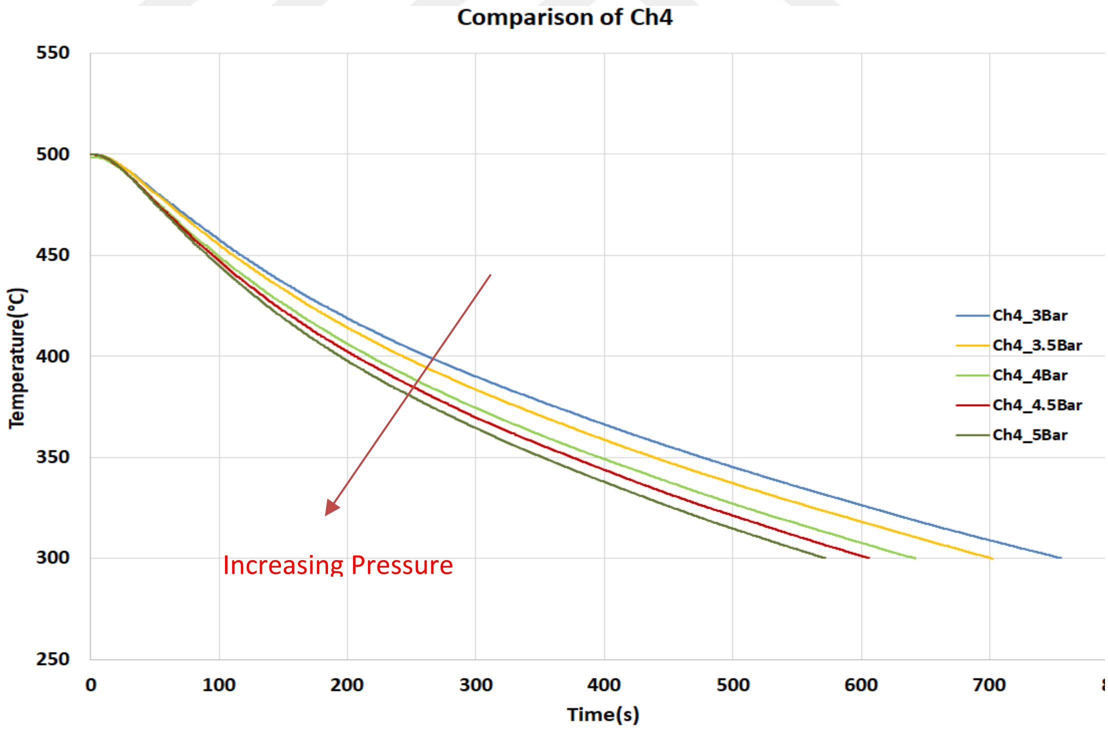

8mm distance at different pressure (Ø2)

Figure 2.29 continues

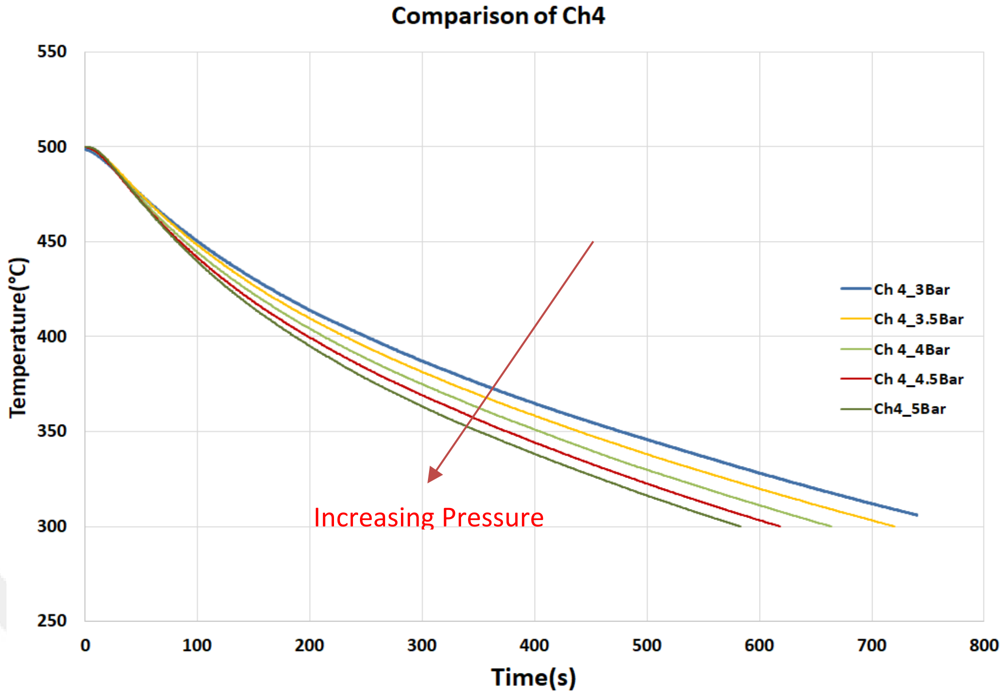

10mm distance at different pressure (Ø2)

Figure 2.29 continues

In Figure 2.28 and 2.29 show that the applied pressure is important. The cooling applied at different distances to the surface is not as effective as the pressure. According to the results, the system Ø4 mm nozzles are cooled 2.5 times earlier than Ø2 mm. In particular, additional Ø2 mm nozzles can be used, where directed solidification is desired and porosity is observed. This cooling system will be less effective than other large-scale nozzles and will prevent the porosity to be observed.

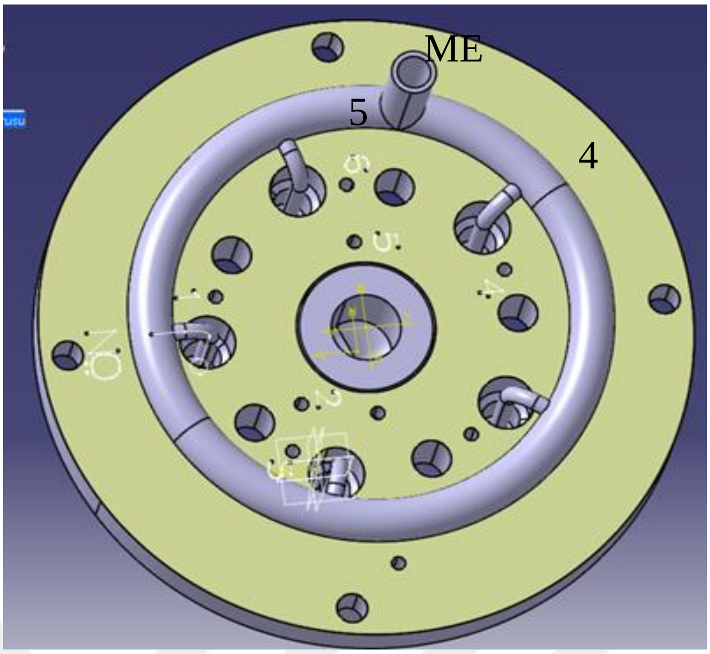

Figure 2.30 Pipe and upper offset mold layout

Figure 2.30 shows the layout of the pipe and upper offset mold. In the industrial field, it is always asked whether the main entrance (ME) is affected the cooling differences between the nozzles, because of the using one entrance. In Figure 2.26 the temperatures of thermocouples show the distribution of temperature are the same at the start and the final of the test.

Studies of surface distance should be made a flat surface with one nozzle, because of control of this system. For this reason, the mathematical model and numerical study will be carried out with the one-single nozzle system.

CHAPTER THREE
NUMERICAL STUDY

In this study, single nozzle studies were designed in the computer. Two-phase simulations were studied with computational fluid dynamics (CFD) to determine the airflow behavior in pipe and heat transfer with mold. Dimensionless values which were defined in section 2.3 were calculated with the results obtained from experiments. In experimental studies, a lot of information about forced convection and air was obtained. And also the obtained information was verified in the simulation program and the mathematical model was designed within the Fluent. For the simulation program, initial conditions were defined. Heat transfer coefficient, cooling time, flow rate of the fluid were defined as an initial conditions.

To eliminate the trial and error methods, castings and other heat transfer problems should be solved in 3D conditions. If the problems are detected during the design of any parts by simulation programs, time and money can be saved. For this reason, there are many researches about simulations. Nowadays, many complex geometry designs can be produced by means of a simulation program without trial and error methods.

In the case of air-cooling, forced convection and natural convection heat transfer correlations are used. This section is focused on model geometry, material properties and boundary conditions.

3.1 Definition of Problem

3.1.1 Mold Geometry and Material Properties

In low pressure castings, generally 1.2344 hot tool work steels are used as mold material. Table 3.1 shows the 1.2344 material properties. (Birleşik Metal, 2019) This material is more cost efficient than other used hot tool work steels. When the material quality-price comparison is made, it is seen that this material is preferred.

Table 3.1 Material properties of 1.2344 hot tool steel

Material Properties	0.40%C 1.10%Si 0.40%Mn 5.10%Cr 1.30%Mo 0.95%V
Material Definition	Having to good thermal conductivity and good thermal resistance - alloy with CrMoV hot tool steel
Scope of Application	Metal injection, extrusion of light metals and used in the production of materials with forging.
Heat Treatment	Normalization °C 1150-850 Softening Annealing 800-820 Delivery Hardness HB30 Max229

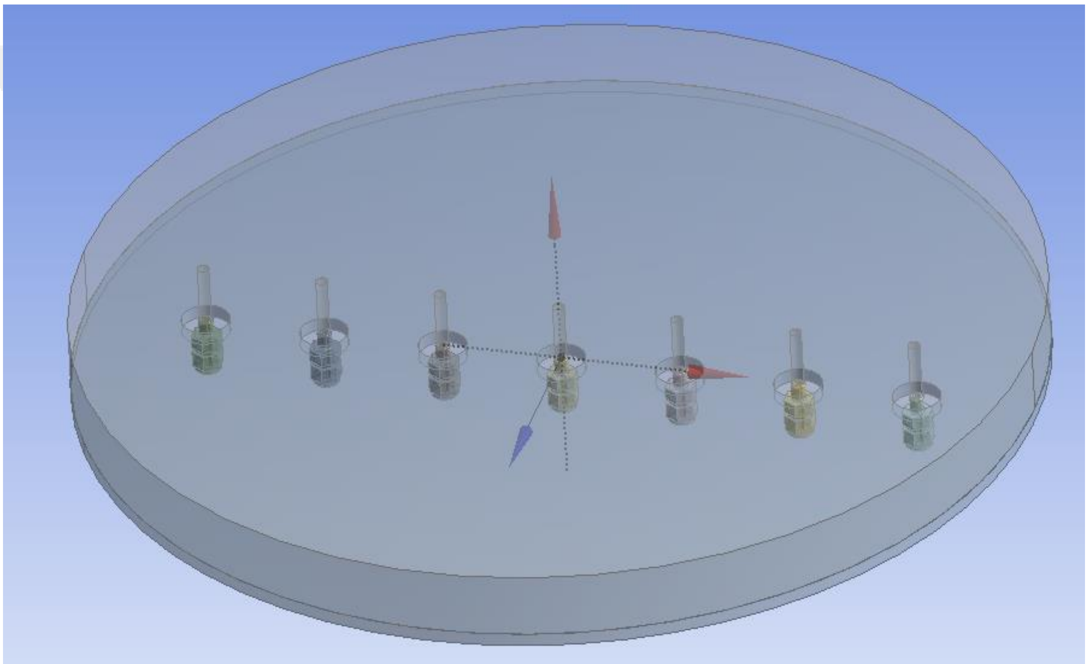

Figure 3.1 Flat plate 1.2344 hot tool steel

Figure 3.1 shows the test plate and thermocouples. The diameter of the flat plate was 430 mm and the height was 25mm. In section 3.3.1, experimental results were given. The test was started when the mold temperature was 400°C and finished at 100°C. In Fluent database, 1.2344 hot tool steel thermal properties are not provided. For this reason, Table 3.2 was used for thermo-physical properties of 1.2344 hot tool steel (Zhang, Maijer & Cockcroft, 2007).

3.1.2 Fluid Properties and Pipe Geometry

Table 3.2 Thermo physical properties of 1.2344 hot tool steel

Thermal Conductivity		Specific Heat		Density
T(°C)	k(W/(m K))	T(°C)	c_p(J/(kg K))	ρ (kg/m^3)
20	24.60	23	458.8	7367
200	26.25	200	518.5	
500	27.30	400	587.8	
600	27.76	600	726.2	
800	28.07	700	905.4	
850	28.39	760	1151.1	

In this study, air was used for fluid. In section 3.2.3, manometer and pressures (Total, static and dynamic pressures) were defined. Due to the calculation of mathematically, read pressures values from manometer were converted the normal values. The term of reading pressure should be detailed before conversion. This is also used for mathematical and numerical calculations.

In Figure 3.2 pressure measurement system is represented. $P_{absolute}$ is the sum of the P_{gauge} and $P_{atmospheric}$ pressure. Gauge pressure is the measure of pressure relative to the ambient atmospheric pressure. When manometer shows a zero value scale means that the absolute pressure of the system is equal to the absolute pressure exerted by the surrounding atmosphere. This should also be taken into account when the numerical calculation. When the numerical calculation is performed, the values entered in the simulation program are defined as the gauge pressure value by the Ansys-Fluent.

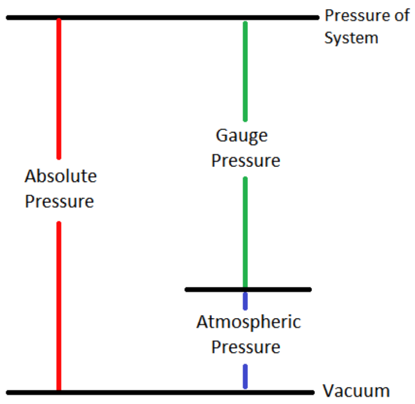

Figure 3.2 Pressure measurement system

Pressures values were read from Testo 6442 flow-meter. In section 2.2.3 working system of Testo 6442 was explained. This manometer works according to DIN ISO 2533. For this reason, pressures values read from flow-meter were converted the working conditions. Test results are shown in Table 3.3. These results show cooling system that Ø4 mm nozzle, 6 mm surface distance, works at different pressures. The system worked average at 20°C and in Figure 3.3 shows working conditions temperature.

Figure 3.3 Temperature value from flow-meter (Personal archive, 2019)

Testo-6442 flow-meter also gives working temperature of the air. Thus, while tests were been carried out, these values were read. In table 3.3 converted values are shown.

Table 3.3 Converted values

Flow-meter values (Nm^3/h)	Pressure (bar)	Working Conditions Flow-Rate (m^3/h)	Working Conditions (m^3/s)
28	3	9.62	0.0027
33	3.5	9.72	0.00269
37	4	9.52	0.00264
42	4.5	9.62	0.00267
46	5	9.49	0.00263

Dimensionless numbers are used to make the properties and classification of air. Dimensionless numbers described in section 1.6.2, when calculating the flow properties of the air, are considered. In the first stage, calculations carried out the compressibility of air and a mathematical calculation carried out about density.

Compressibility of the fluid is decided with the Mach number. (Mach number is explained at 1.6.2 Dimensionless Number section). From equation 2.9; $M = V_{object} / V_{sound}$, V_{sound} is the velocity of sound in air is calculated from equation 2.10, this equation gives the average speed of sound for given temperature and for 293,15K ambient temperature V_{sound} is calculated 343 m/s. And now another value for 2.9 equation value V_{object} is calculated from volume flow or mass-flow. The mass-flow rate is calculated for the comparison of simulation and experimental results. The cooling system and name of boundaries are shown in Figure 3.4. Boundary conditions consist of Ø16 mm inlet diameter, wall and Ø4 mm outlet diameter.

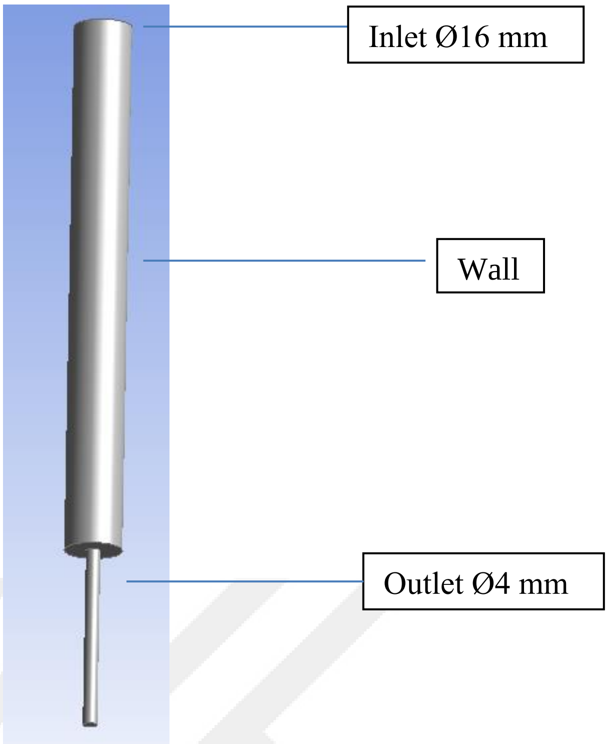

Figure 3.4 Nozzle geometry

V_{object} is calculated from volumetric flow rate:

$$Q = A\,V \tag{3.1}$$

In this equation Q (m^3/s) is volumetric flow-rate. A (m^2) is an area of the pipe. From equation 4.1 inlet air velocity is 13.29 m/s and outlet air velocity is calculated 212.72 m/s. Outlet velocity is calculated from mass conservation. For the outlet velocities, necessary results will be obtained from simulation. This value will give us preliminary information to be used in the setup section of the simulation program. Finally, from equation 2.9, the Mach number is calculated 0.62.

In section 1.6.2, compressibility was associated with this speed and the Mach number. If the fluent velocity is higher than 100 m/s or Mach number is higher than 0.3, fluent is compressible or it means that air density could change above 5 percent. Therefore, our cooling system can be categorized as compressible or density change flow. Experimental test were conducted different pressures. To calculate density, equation 3.2 is used;

$$\rho_{air} = \frac{P}{R\,T} \tag{3.2}$$

In this equation, $\rho_{dry\text{-}air}$ is the density of air (kg/m^3), P is air pressure (Pa), R is specific gas constant for dry air (287.05 J/ (kg K)), T is temperature (K). The density values calculated for the different pressures are given in table 3.4.

Table 3.4 Dry air densities for different pressures

Flow-meter values (Nm^3/h)	**Pressure (bar)**	**Working Conditions Flow-Rate(m^3/s)**	**Mass flow ($\dot{m}$ - kg/s)**	**Density Air ($\rho_{dry\text{-}air}$)**
28	3	0.00267	0.00953	3.565
33	3.5	0.0027	0.01123	4.159
37	4	0.00265	0.01259	4.754
42	4.5	0.00268	0.01429	5.348
46	5	0.00264	0.01565	5.942

To calculate mathematical and numerical study another important dimensionless number which is Reynolds number is calculated from Equation 2.8. In this equation dynamic viscosity is calculated from the following Sutherland's equation.

$$\mu = \frac{1.458x10^{-6}T^{1.5}}{T + 110.4} \tag{3.3}$$

In this equation, T is 293.15 K and μ is calculated as 1.813405x10^{-5} N s/m^2.

3.2 Numerical Results

Simulation steps consist of pre-processing (geometry design and mesh structure), solver (fluent setup) and post-processing (display result) and are shown in Figure 3.5.

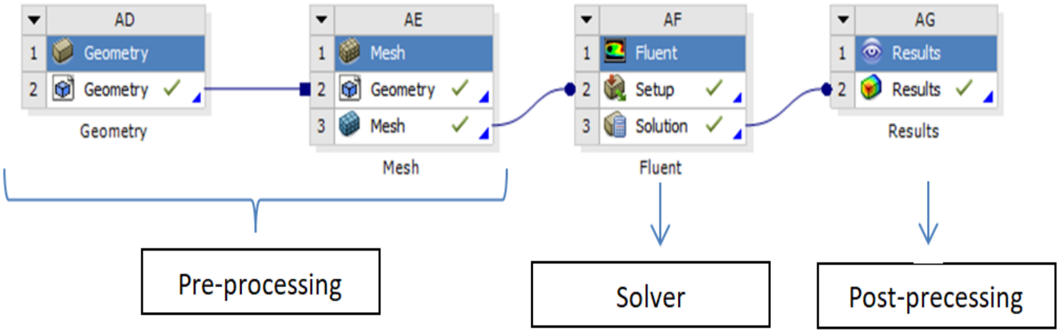

Figure 3.5 Steps of simulation study

3.2.1 One-Single Pipe Numerical Setup and Results

3.2.1.1 Geometry Design

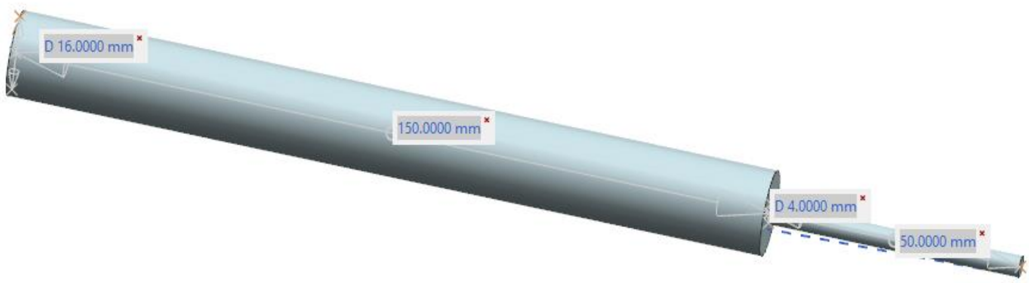

Figure 3.6 Geometry design

In Figure 3.6 shows geometry design which consists of two different cylinders. The first cylinder is defined inlet which is designed as Ø16 mm diameter and 150 mm length and the second cylinder is defined outlet which is designed as Ø4 mm diameter and 50 mm length.

3.2.1.2 Mesh Structure

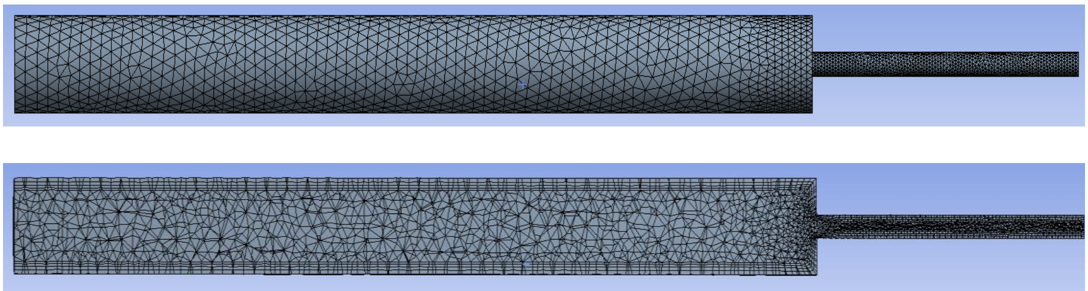

Figure 3.7 General view of mesh

In Figure 3.7 shows the general view of the mesh. In our system, unnecessary geometries hadn't been drawn in order not to create a mesh crowd. It has been found that these details are not effective with many simulations. Therefore, the drawn region was taken from the place behind the flow measurement location. And also the section of pipe and inflation are shown. Details of inflation are shown in Figure 3.8. Inflation is critical to the accuracy and capture of flow physics near the wall when using CFD calculation. Boundary layers are defined in section 1.6.1.4.

Scope	
Scoping Method	Geometry Selection
Geometry	1 Body
Definition	
Suppressed	No
Boundary Scoping Method	Geometry Selection
Boundary	3 Faces
Inflation Option	Total Thickness
Number of Layers	4
Growth Rate	0.8
Maximum Thickness	2.0 mm
Inflation Algorithm	Pre

Figure 3.8 Details of inflation

Mesh was occurred from 21592 nodes and 51010 elements. Skewness and orthogonal quality are an important quality factor. So when the mesh is checked, these quality factors should be controlled.

Skewness should be less than 0.9 and orthogonal quality should be close to 1. In Figure 3.9 mesh quality is shown.

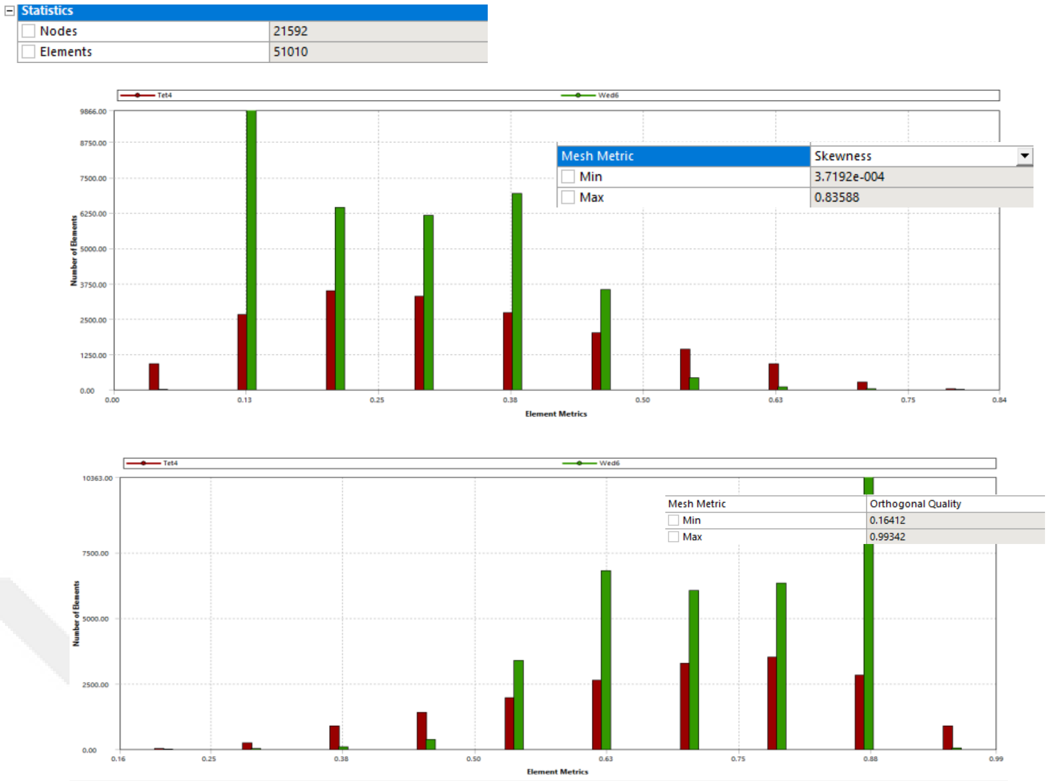

Figure 3.9 Details of mesh quality

3.2.1.3 Solver Ansys Fluent

Pressure based solver uses a projection method. This method provides take momentum and pressure-pressure correction. Pressure-velocity coupling algorithms are derived by reformatting the continuity equation. This solvent can be used for both low speeds and high speeds. Therefore, it provides flexibility in the solution.

The k-epsilon model is one of the most common used turbulence models. In the literature review, this model has been used in many studies. However, this model is a problem in reverse pressure gradients. In this case, it does not give the desired performance. Sometimes, the same situations were observed in our study.

3.2.1.3 Results

In Table 3.4, dry air densities for different pressures are shown. The mathematical solutions of the inlet and outlet velocities obtained from these values and values are shown in Table 3.5. Outlet velocities were calculated from mass conservation.

$$\dot{m} = \rho V A \tag{3.4}$$

In this equation, $\dot{m}$ is the mass flow-rate (kg/s), V is velocity of fluent (m/s), ρ is the density of fluent kg/m^3 and A is the diameter of the pipe (m) where the fluent crosses. The conservation of mass is a fundamental concept of physics. For this reason, inlet and outlet mass flow-rate must be same and we can calculate velocity of fluent at the inlet and outlet mathematically.

Table 3.5 Inlet and outlet velocity mathematical solutions at different pressures

Pressure (bar)	Velocity (m/s)	
	Inlet	Outlet
3	13.29	212.62
3.5	13.42	214.79
4	13.17	210.72
4.5	13.29	212.62
5	13.10	209.58

According to outlet results, turbulent model was applied to the simulation.

Velocities of mathematical and simulation results are shown in Table 3.6. These results show that the deviation in outlet velocities is high.

Table 3.6 Inlet and outlet mass flow-rate mathematical and simulation results at different pressures

Pressure (bar)	Mass Flow Rate					
	Inlet			Outlet		
	Maths Result	Simulation Result	Deviation Ratio (%)	Maths Result	Simulation Result	Dev. Rat. (%)
3	0.0096	0.0092	3.86	0.0096	0.0092	3.86
3.5	0.0113	0.0107	5.26	0.0113	0.0107	5.26
4	0.0126	0.0121	4.5582	0.0126	0.0121	4.56
4.5	0.0143	0.0133	6.975	0.0143	0.0133	6.98
5	0.0156	0.0143	8.788	0.0157	0.0143	8.79

*Maths refers to mathematical calculation.

In table 3.6 shows the mathematical and simulation mass flow rate at different pressures. The mass flow-rates which were obtained by simulations were checked. These results were quite consistent. It also closely matches the mathematical results we have made. These results are shown in Figure 3.10.

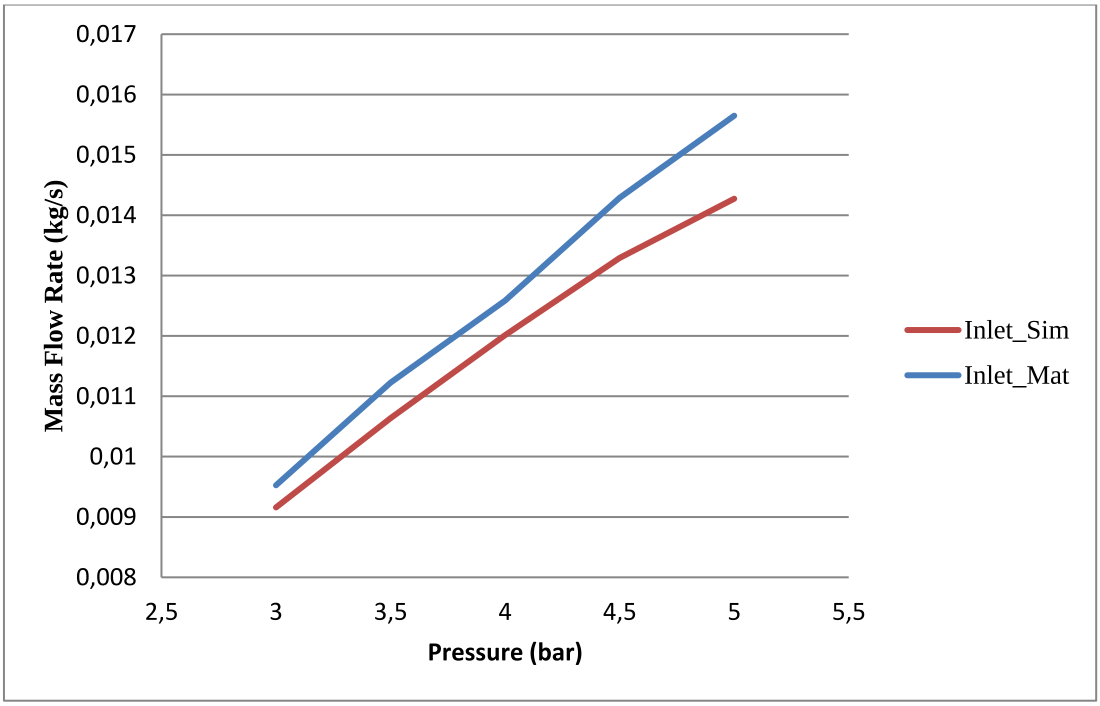

Figure 3.10 Comparison of inlet mass flow rate (Simulation&mathematical)

The distributions of velocities are shown in Figure 3.11. The velocity of the fluid has increased after entered the Ø4 pipe.

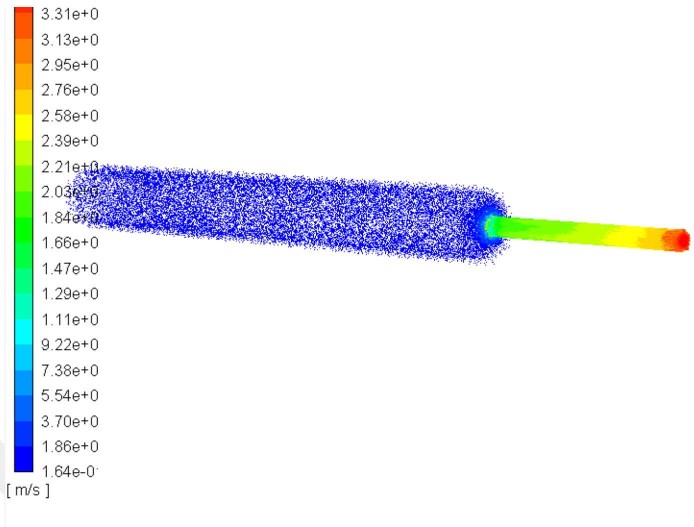

Figure 3.11 Distributions of velocities

The values which obtained from the simulation, were used for the flat plate simulation. After this section, flat plate simulations were investigated.

3.2.2 Flat Plate Numerical Setup and Results

In Figure 3.1, geometry of flat plate is shown. 1.2344 hot tool steel was used for experimental test and physical properties of 1.2344 are given in Table 3.2.

3.2.2.1 Mesh Structure

Figure 3.12 General view of simulation view

Figure 3.12 shows the simulation zone. Mesh size structure affects the results. Reducing the mesh structure allows us to achieve a more accurate result. However, this will extend the solution time. Our plate is a round and flat surface, so simulations can work with 2D. 2D axisymmetric includes the prediction of the circumferential or swirl velocity.

System was solved with density-based and transient system. Because of the temperature changes over time, the system was designed as transient.

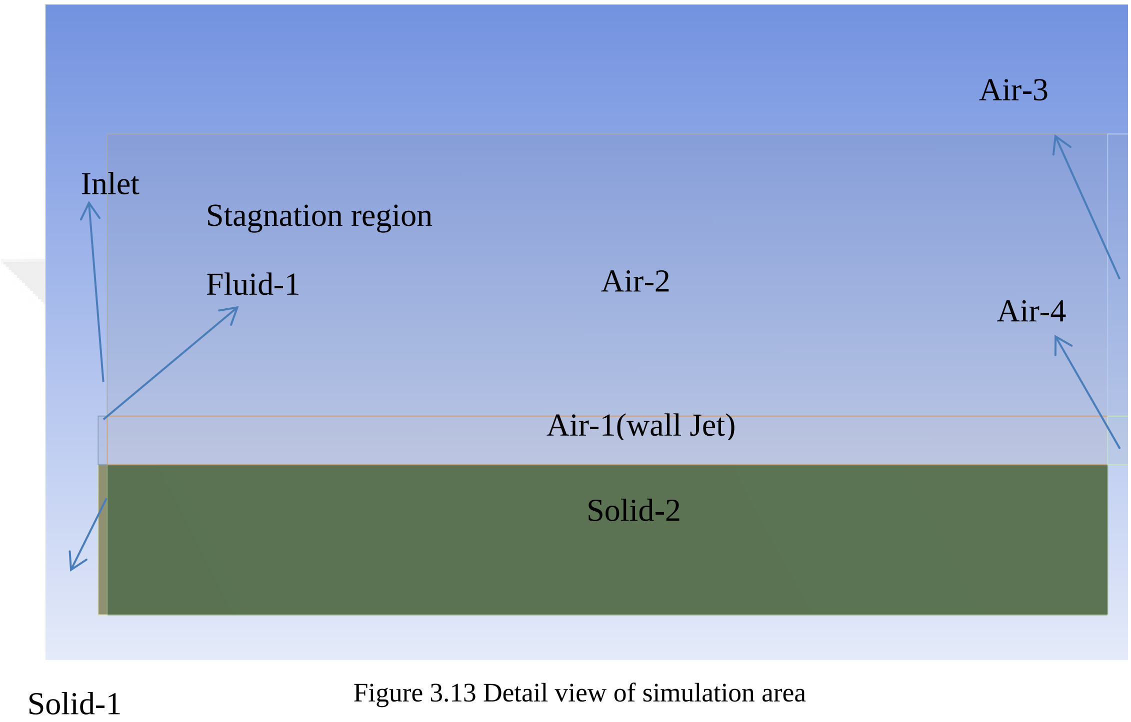

Figure 3.13 Detail view of simulation area

In Figure 3.13 shows the detail view of simulation area. Different regions of a jet impingement flow are shown in Figure 1.19. Similar regions are designed for the simulation. The forced air enters the area through the called as Inlet which is the outlet of the pipe. Fluid-1 is represented as Stagnation Region. Forced air crosses Fluid-1 and strikes the flat plate. Flat plate occurs from Solid-1 and Solid-2. Surrounding air is divided as Air-1, Air-2, Air-3 and Air-4.

The mesh system according to this design is shown in Figure 3.14.

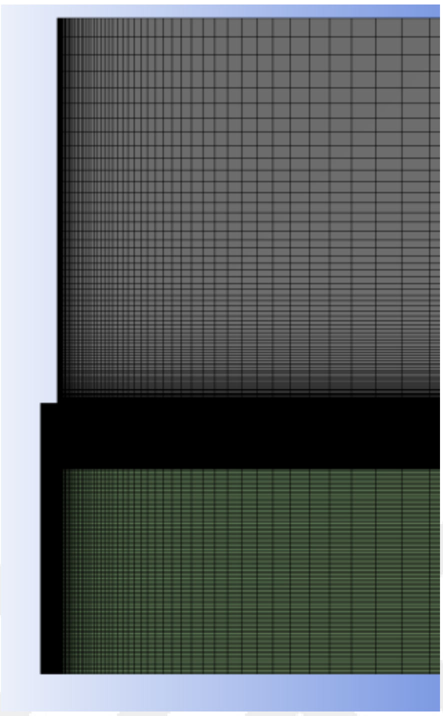

Figure 3.14 Detail of flat plate mesh

The pipe design is the same as the previous section. The pipe diameter is Ø4 mm. In the previous system, the output is defined here as the input. The environment has been expanded as much as possible. The environment is divided into 4 sections. Emissivity was taken 0.7.

3.2.2.2 Results

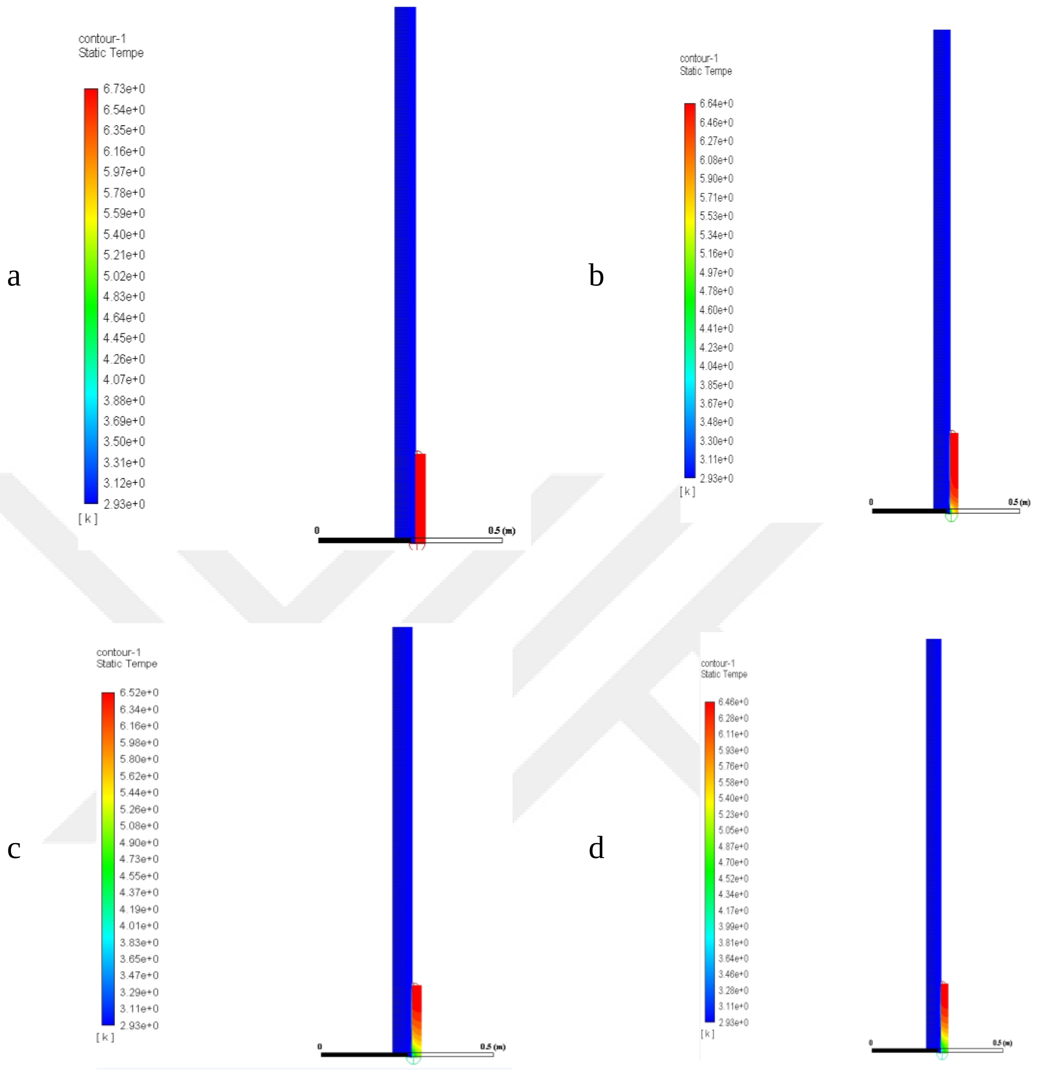

Figure 3.15 Simulation test results

Figure 3.15 shows the simulation test results. The simulation was started at 400°C. The system was set depending on time. The operating time is set to 6 min 5s. Figure 3.15a shows the starting conditions of the simulation. Figure 3.15 b and 3.15c show the simulation results at 3 and 5 minutes. Figure 3.15d shows the end of the simulation.

Figure 3.16 shows the simulation and experimental results on channel 4. In the simulation, the location of the thermocouple is located in the same place as the experimental setup. Result trends are very close to each other. One of the reasons for temperature differences is that the heat in the Protherm device had not been discharged. In addition, the development of simulation studies should be continued.

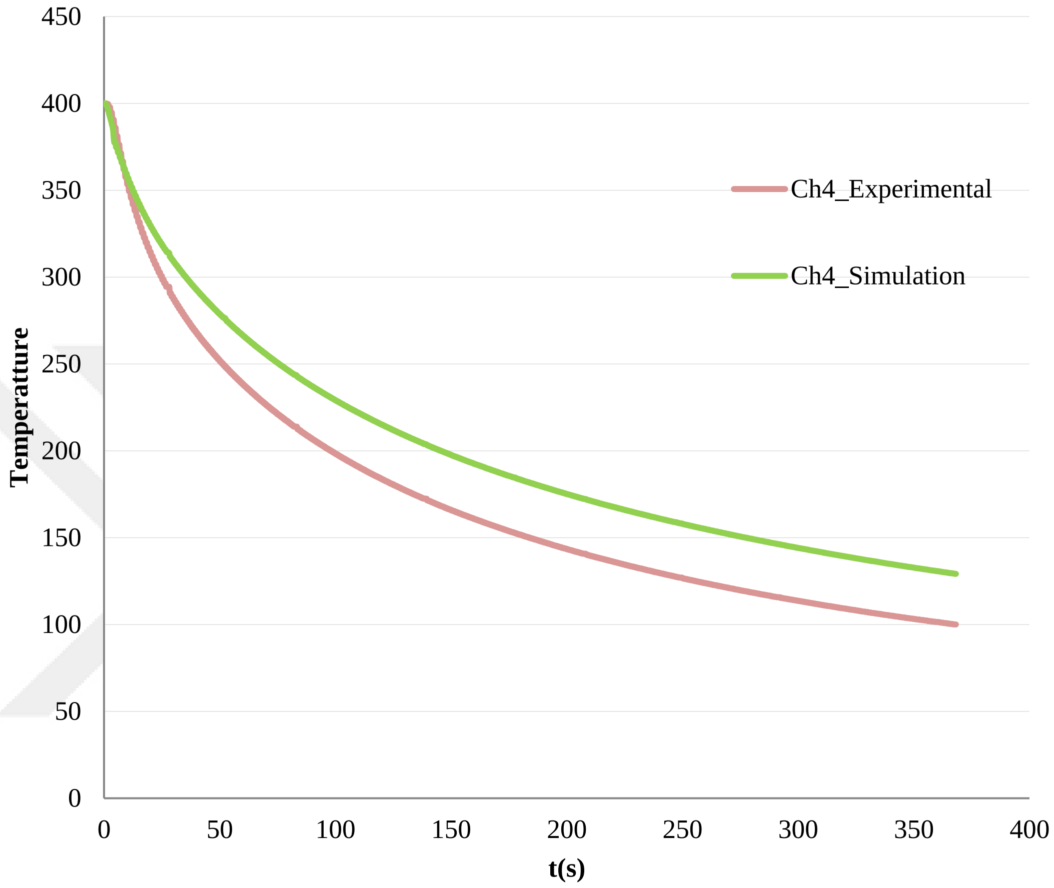

Figure 3.16 Comparison of Ch4 temperature

CHAPTER FOUR
CONCLUSION AND FUTURE WORK

Due to the lightweight and durability of aluminum, its usage area is increasing day by day. Cooling is an important parameter for casting. By means of cooling, directed solidifications and improvements in the internal structure are achieved.

In the multiple nozzle experimental study, Ø2 mm and Ø4 mm diameter tests showed that different types of cooling systems are very effective in air consumption. And in the industrial field, it is always asked whether the main entrance is affected the cooling differences between the nozzles, because of the using one entrance. The temperatures of thermocouple show the distribution of temperature are the same at the start and the final of the test. The obtained results are showed that the applied pressure is important. The cooling applied at different distances to the surface is not as effective as the pressure. Studies of surface distance should be made a flat surface with one nozzle, because of control of this system. Also, the other important issue relates to the nozzle diameter. According to the results, the system Ø4mm nozzles are cooled 2.5 times earlier than Ø2mm. Additional Ø2mm nozzles can be used, where directed solidification is desired and porosity is observed. This cooling system will be less effective than other large-scale nozzles and will prevent the porosity to be observed.

A single nozzle system of Ø4 mm and 6 mm were used in the simulation studies. Simulation studies were examined in two sections. First, the flow in the pipe was examined. This system worked on pressure-based and K-epsilon model. This model is a problem in reverse pressure gradients. There were some errors during the simulation studies. The fluid has lost a high pressure at the inlet from Ø16 mm to Ø4 mm. The speed of exit from the nozzle exceeds the speed of sound. Output speed varies between 320-330 m/s. The mass conservation principle should be considered when simulation works. Secondly, cooling was carried out on a flat surface. The test plate was a round and flat surface, so simulations could work with 2D. 2D axisymmetric includes the prediction of the circumferential or swirl velocity. This gave us a faster solution. If the studies are verified in the simulation, the number of trial and error during production will be reduced. This will save us money and time. Observing the problems during the design phase and responding to them immediately will provide better quality products.

REFERENCES:

Abdullah, M. F., Zulkifli, R., Harun, Z., Abdullah, Z., & Ghopa., W.A.W. (2018). Experimental and numerical simulation of the heat transfer enhancement on the twin impingement jet mechanism. *Energies, 11*(4), 927.

Akçay, M., Yazıcı, H., Gölcü M., Köseoğlu. M. F., Sekmen Y. (2011). Oto Cam Temperleme İşlemindeAni Soğutma SırasındaMeydana Gelen Isı Transferinin Deneysel Olarak İncelenmesi. *6th International Advanced Technologies Symposium, 6,* 194-199.

Anuj, K. S., & Anupam, D. (2017). Flow and thermal characteristics of jet impingement: Comprehensive review. *International Journal Of Heat And Technology, 35,* 153-166.

Azimi, A., Ashjaee, M., & Razi, P. (2015). Slot jet impingement cooling of a concave surface in an annulus. *Experimental Thermal and Fluid Science, 68*, 300–309.

Baughn, J.W., Hechanova, A. E., Yan, X. (1991). An experimental study of entrainment effects on the heat transfer from a flat surface to a heated circular impinging jet. *Heat Transfer, 113,* 1023–1025.

Birleşik Metal, (2019). *Material properties of 1.2344*. Retrieved May 06, 2019, from https://www.birlesikmetal.com.tr/assets/Files/BirlesikMetalKitap.rar.

Cengel, Y. A., Cimbala, C. M., & Turner, R. H. (1998). *Heat transfer. A practical approach*. New York: McGraw-Hill.

Chandramohan, P., Murugesan, S. N., Arivazhagan, S., (2017). Heat transfer analysis of flat plate subjected to multi- jet air impingement using principal component analysis and computational technique. *Journal of Applied Mechanics*, *10*, 293-306.

Dharavath, M., & Chakraborty, D. (2013). Numerical simulation of supersonic jet impingement on inclined plane. *Defence Science Journal, 63*(4), 355-362.

Guofa M., Xiangyu L., Kuangfei W., & Hengzhi, F. (2009). Numerical simulation of low pressure die-casting aluminum wheel. *China Foundry*, *6*(1), 48-52.

Helms, H., & Lambrecht, U. (2007). The potential contribution of light weighting to reduce transport energy consumption. *The International Journal of Life Cycle Assessment*, *12* (1), 58-64.

Jambunathan, K., Lal, E., Moss, M. A., & Button, B. L. (1992). A review of heat transfer data for single circular jet impingement. *International Heat and Fluid Flow*, *13*, 106 - 115.

Hines, A. J. (2004). Determination of interfacial heat-transfer boundary conditions in an aluminum low-pressure mold test casting. *Metallurgical and Materials Transactions*, *35*(2), 299–311.

Koseoglu, M. F., & Baskaya, S. (2010). The role of jet inlet geometry in impinging jet heat transfer, modeling and experiments. *International Journal of Thermal. Sciences*, *49*, 1417-1426.

Lasance, C. J. M. (1997). *Heat transfer coefficient.* Retrieved May 06, 2019, from https://www.electronicscooling.com/2005/11/advancesinhighperformancecooling _for-electronics/

Lee, H. J. R. (2006). *Effect of cooling circuit duration on formation of solidification shrinkage in A356 casting automotive wheels.* Master Thesis, Aukland University, Aukland.

L&ES. (2014). *Low pressure die casting*. Retrieved April 03, 2019, from http://landesolutions.com/index.php?m=content&c=index&f=show&catid=12&l=1&id=38

Mishra, P. (2016). *Difference between laminar and turbulent flow.* Retrieved March 20, 2019, from https://www.mechanicalbooster.com/2016/08/difference-between-laminar-and-turbulent-flow.html

Marzec K., & Marzec K. (2014). Heat transfer characteristic of an impingement cooling system with different nozzle geometry. *Journal of Physics: Conference Series, 530*, 1-9.

Moayedinia, S. (2014). *Quantification of cooling channel heat transfer in low pressure die casting*, Master Thesis, University of British Columbia, Vancouver.

Molana M., & Banooni S. (2013). Investigation of heat transfer processes involved liquid impingement jets. *Brazilian Journal of Chemical Engineering, 30*, 0104-6632.

Mr. S K Muttagi , Dr. Geetanjali V Patil, Dr. Suneelkumar N Kulkarni, & Mr.Vishwanath. (2015). Interface heat transfer coefficient between casting and round chilled moulds during solidification of aluminium alloy castings. *International Journal of Engineering Research & Technology (IJERT), 4*(3), 341-346.

Rappa, M., Drezet, J., Gremaud, M. A (1999). New hot-tearing criterion. *Metallurgical and Materials Transaction , 30*(2),449-455

Royne, A., & D, Ch. (2006). Effect of nozzle geometry on pressure drop and heat transfer in submerged jet arrays. *International Journal of Heat and Mass Transfer, 49*, 800-804.

Singh, D. Premachandran, B., & Kohli, S. (2013). Experimental and numerical investigation of jet impingement cooling of a circular cylinder. *International Journal of Heat and Mass Transfer*, *60*, 672–688.

United Nations Environment Programme (UNEP), (2019). *Sustainable transport and air pollution*. Retrieved April 02, 2019, from https://www.unenvironment.org/explore-topics/resource-efficiency/what wedo/cities/ sustainable -transport-and-air-pollution.

Wang, Y. (2014). Optimization of low-pressure die casting process parameters for reduction of shrinkage porosity in ZL205A alloy casting using Taguchi method. *Proceedings of the Institution of Mechanical Engineers Part B Journal of Engineering Manufacture*, *228*(11), 1508-1514

Wei, X. (2014). *Thermal mechanical analysis of interfacial behavior in aluminum alloy wheel casting process*. Master Thesis, Zhejiang University, Hangzhou.

Whelan, B. & Robinson, A. (2009). Nozzle geometry effects in liquid jet array impingement. *Applied Thermal Engineering*, *29*, 2211-2221.

Zhang, B., Maijer, D., & Cockcroft, S. (2007). Development of a 3-D thermal model of the low-pressure die-cast (LPDC) process of A356 aluminum alloy wheels. *Materials Science and Engineering, 464*(1), 295-305.

Zhang, B., Cockcroft, S., Maijer, D., Zhu, J., Phillion, A. (2005). Casting defects in low-pressure die-cast aluminum alloy wheels. *The Journal of The Minerals, Metals & Materials Society*, 57(11), 36-43.

Zhu, J., Cockcroft, S., Maijer, D. (2006). Modeling of microporosity formation in A356 aluminum alloy casting. *Metallurgical and Materials Transactions, 37*(3), 1075-1085.

Zukowski, M. (2013). Heat transfer performance of a confined single slot jet if air impinging on a flat surface. *International Journal of Heat and Mass Transfer, 57*, 484-490.